



A cosmogenic nuclide-derived chronology of pre-Last Glacial Cycle glaciations during MIS 8 and MIS 6 in northern Patagonia

Tancrede P. M. Leger¹, Andrew S. Hein¹, Ángel Rodés², Robert G. Bingham¹, Irene Schimmelpfennig³,
5 Derek Fabel², Pablo T. Gonzalez⁴, ASTER Team⁺

¹ School of GeoSciences, University of Edinburgh, Drummond Street, Edinburgh, EH8 9XP, UK

² Scottish Universities Environmental Research Centre, Scottish Enterprise Technology Park, East Kilbride, G75 0QF, Glasgow, UK

10 ³ Aix-Marseille Université, CNRS, Coll. France, IRD, INRAE, CEREGE, Aix en Provence, 13545, France

⁴ Instituto de Geografía, Facultad de Historia, Geografía y Ciencia Política, Pontificia Universidad Católica de Chile, Santiago, Chile

⁺ A full list of authors appears at the end of the paper.

15 *Correspondence:* Tancrede P. M. Leger (Tancrede.leger@ed.ac.uk)

Abstract. The precise environmental mechanisms controlling Quaternary glacial cycles remain ambiguous. To address this problem, it is critical to better comprehend the drivers of spatio-temporal variability in ice-sheet evolution by establishing reliable chronologies of former outlet-glacier advances. When spanning multiple glacial cycles, such chronologies have the capacity to resolve conundrums on interhemispheric phasing of glaciations and climate events. In southern Argentina, reconstructions of this kind are achievable, as Quaternary expansions of the Patagonian Ice Sheet have emplaced a well-preserved geomorphological record covering several glacial cycles. Moreover, robust ice-sheet reconstructions from Patagonia are powerful barometers of former climate change, as Patagonian glaciers are influenced by the Southern Westerly Winds and its coupled Antarctic Circumpolar Current. Former shifts in these circulation mechanisms are essential to better constrain, as they may have played a critical role in pacing regional and possibly global Quaternary climate change. Here, we present a new set of cosmogenic ¹⁰Be and ²⁶Al exposure ages from pre-Last Glacial Cycle moraine boulder, glaciofluvial outwash cobble and bedrock samples. This dataset constitutes the first direct chronology dating pre-LGM glacier advances in northern Patagonia, and completes our effort to date the entire preserved moraine record of the Río Corcovado valley system (43°S, 71°W). We find the outermost margins of the study site depict at least three distinct pre-Last Glacial Cycle glaciations occurring at 284 ± 7 ka, 257 ± 7 ka, and 147 ± 4 ka. Combined with the local LGM chronology, we discover that a minimum of four distinct Pleistocene glaciations occurred during Marine Isotope Stages eight, six, and two in northern Patagonia. Evidence for stage four and three deposits were not found at the study site, which illustrates former longitudinal and latitudinal asynchronies in Patagonian Ice Sheet mass balance during these stages. We find the most extensive middle-to-late



35 Pleistocene expansions of the Patagonian Ice Sheet appear to be out-of-phase with local summer insolation intensity, but
synchronous with orbitally-controlled periods of longer and colder winters. Our findings thus enable to explore the potential
roles of seasonality and seasonal duration in driving southern mid-latitude ice-sheet mass balance and facilitate novel glacio-
geomorphological interpretations for the study region. They also provide empirical constraints of former ice-sheet extent and
dynamics that are essential to calibrating numerical ice-sheet and glacial isostatic adjustment models.

40

45

50

55

60



65 1 Introduction

Understanding the environmental mechanisms driving the Quaternary build-up and collapse cycles of Earth's major ice sheets remains a focus of ongoing research. Key to this research is the establishment of detailed chronologies offering direct dating of major ice-sheet expansion and recession events (Darvill *et al.*, 2016). Numerical glacier chronologies are most
70 informative when presenting unambiguous dating of ice-sheet margins spanning the entirety of the last glacial cycle (LGC) and ideally earlier Quaternary glacial cycles (Kaplan *et al.*, 2010; Schaefer *et al.*, 2015). To the east of the Patagonian Andes, the Argentinian foreland contains one of the most complete and well-preserved sequences of Quaternary glacial deposits in the world (Clapperton, 1993). This unique geomorphological record provides the opportunity to reconstruct and date glacier
75 fluctuations of the formerly 2500 km-long (from north to south) Patagonian Ice Sheet (PIS) over several glacial cycles (Mercer, 1976, Hein *et al.*, 2011). Furthermore, the PIS occupied a key mid-latitude position in the ocean-dominated Southern Hemisphere (SH) and was the only ice mass to fully intersect the precipitation-bearing southern westerly wind (SWW) belt; a fundamental feature of the southern mid-latitude climate system. Hence, reconstructing the timing of PIS expansion and recession events during several glacial cycles can provide rare insight into southern mid-latitude Quaternary climate evolution (Davies *et al.*, 2020).

80 Palaeo-climate proxy records such as those retrieved from ice- and ocean-sediment cores indicate that some of the most potent Quaternary cooling events occurred during the Middle Pleistocene (Parrenin *et al.*, 2013; Shakun *et al.*, 2015), a period (~800 - 130 ka; Hughes *et al.*, 2020) characterized by 100-ka pacing of glacial-interglacial cycles. Paradoxically, there is a dearth of directly-dated terrestrial glacial records for these glacial events (Hughes *et al.*, 2020). In Patagonia,
85 bracketing ages for pre-LGC glaciations have been produced in some places (*e.g.* near Lago Argentino; 50.5°S) with $^{40}\text{Ar}/^{39}\text{Ar}$ dating, *K-Ar* dating, and palaeo-magnetic measurements on lava flows interbedded between Pliocene/Pleistocene glacial-till units (Mercer, 1976; Sylwan *et al.*, 1991; Meglioli, 1992; Singer *et al.*, 2004). For instance, Mercer (1976) used such methods to constrain the likely timing of the Greatest Patagonian Glaciation to between 1.2 Ma and 1.0 Ma in the Río Gallegos (52°S) and Lago Buenos Aires (46.5°S) regions. While such studies have been instrumental in establishing the
90 broad chronological framework for Patagonian glaciations (Rabassa and Coronato, 2009), direct numerical dating of individual outlet-glacier advances is now required to develop detailed knowledge of pre-LGM and pre-LGC ice-sheet activity in Patagonia.

In Patagonia, direct numerical dating of pre-LGC glacial advances, achievable using terrestrial cosmogenic nuclide (TCN) surface exposure dating, has been limited to two valleys of eastern central Patagonia (Kaplan *et al.*, 2005; Hein *et al.*, 2009; 2011; 2017; Cogež *et al.*, 2018). Throughout the rest of the southern mid-latitudes (23 - 66 °S), terrestrial glacial records yielding TCN exposure ages that pre-date the LGC have been reported using moraine boulders in New Zealand (Putnam *et*



100 *al.*, 2013), the southern central Andes (Terrizzano *et al.*, 2017) and Tasmania (Barrows *et al.*, 2002; Kiernan *et al.* 2004;
2010; 2014; 2017; Colhoun and Barrows, 2011, Augustinus *et al.*, 2017). Because pre-LGC moraines and boulders are often
105 poorly preserved, the majority of these investigations have identified the approximate timing of individual pre-LGC glacial
advances with small ($n = 5$ per moraine) and scattered sets of ages. Consequently, robust and direct numerical
chronologies of pre-LGC glacial expansion events remain particularly scarce in the southern mid-latitudes. Patagonian
investigations have shown that TCN exposure dating can yield direct ages for the deposition of pre-LGC moraine-outwash
110 complexes preserved in the Argentinian steppe (*e.g.* Hein *et al.*, 2017). While moraine boulders are well-suited to dating
glacier advances of the LGC, Hein *et al.* (2009) revealed that targeting outwash terraces in eastern Patagonia can be more
appropriate for dating pre-LGC glacial margins, because their low-gradient surfaces are less prone to degradation via
gravity-driven diffusion when compared to steep-sided and unconsolidated moraines. On pre-LGC moraines, such
degradation more frequently causes moraine surface lowering and boulder exhumation post-deposition, leading to significant
115 exposure-age scatter and underestimations of moraine formation age. In contrast, surface cobbles from well-preserved
outwash plains tend to display comparatively less post-depositional scatter and are thought to date the glacial event more
closely (Hein *et al.*, 2009). This approach has been used successfully to constrain the timing of glacial advances in several
locations of central and southern Patagonia (Darvill *et al.*, 2015; Hein *et al.*, 2009; 2011; 2017; Mendelová *et al.*, 2020).
However, to date, no pre-LGC glacial events have been dated using this technique in northern Patagonia. Consequently, here
we adopt this approach and target both moraine boulders and outwash surface cobbles to constrain the timing of pre-LGC
glacial advances in northeastern Patagonia.

We focus our investigation on the Río Corcovado (RC) valley system (43°S; 71°W), formerly host to a major outlet glacier
of the PIS in northeastern Patagonia (Caldenius, 1932). We present a multi-glacial-cycle ^{10}Be and ^{26}Al TCN exposure-age
120 chronology from the three stratigraphically oldest glacial moraine/outwash complexes deposited by the RC outlet glacier.
This study builds on our earlier work (Leger *et al.*, 2020, 2021a,b) to compile a geochronological reconstruction that spans
the entire preserved moraine-outwash record of the RC valley system. We use our cosmogenic nuclide-derived chronology
to test whether major middle Pleistocene advances previously dated in central Patagonia (Hein *et al.*, 2009; 2017) coincide
with moraines found in its northeastern sector (this study), and thus whether such advances depict strong regional climate
signals expressed across much of the palaeo-ice front. We then compare the different magnitudes of middle Pleistocene
125 Patagonian glaciations relative to other formerly glaciated regions of the world, and thereby assess the presence of former
interhemispheric and inter-regional *a/synchronies* in ice-sheet behaviour. Finally, we evaluate the synchronicity of PIS
expansion events with other global and regional palaeo-climate proxy records, and explore the potential role of various
insolation parameters on controlling middle-to-late Pleistocene climate variations in Patagonia and the southern mid-
latitudes.

130



2 Setting

Our study site focuses on the ice-marginal environment of the former PIS during Quaternary ice-age maxima, at the latitude of its major eastward-flowing Palena outlet glacier (43°S; Leger *et al.*, 2020; 2021a). This up to 100 km-long outlet glacier
135 diverged towards the eastern mountain front into three glaciers occupying the Río Frío valley to the northeast, the Río
Huemul (RH) valley to the east, and the RC valley to the south (Fig. 1; Leger *et al.*, 2021a). The local valleys are
characterised by a westward-sloping bed topography such that the former outlet glaciers flowed up along reverse-sloping
beds. The surface geology of the study area is characterised by well-preserved and distinct sequences of ice-contact
glaciogenic deposits interspersed among their associated glaciolacustrine and glaciofluvial sediment-landform assemblages
140 (Leger *et al.*, 2020). Terminal moraine complexes indicate that the RC and RH outlet glaciers re-converged to deposit
moraine sequences located approximately 60 km to the east of the Argentinian town of Corcovado (43°54'S; 71°46'W), into
an environment presently climatically defined as the semi-arid Patagonian steppe (Fig. 1; Garreaud *et al.*, 2013). Local
aridity (~570 mm a⁻¹; Fick and Hijmans, 2017; Fig. 1a) results from the Patagonian Andes acting as a powerful orographic
barrier to the dominant SWW (Fig. 1a), causing a potent west-east rain-shadow effect (Garreaud *et al.*, 2013; Fig. 1a). Along
145 the flowlines of the RC outlet glacier, ice flow eroded bedrock mainly sourced from the Mesozoic north Patagonian batholith
towards the west (Hervé *et al.*, 2017) along with formations of Jurassic/Cretaceous volcanic and sedimentary units located
further east (Haller *et al.*, 2003). Moraine-outwash complexes studied here thus contain a mixture of rock types including
quartz-bearing leuco-monzonite, granite and white granodiorite that are well-suited to TCN exposure dating using *in situ*
¹⁰Be and ²⁶Al radionuclides.

150
Ice sheet-wide geomorphological mapping of glacial sediment-landform assemblages has been conducted by Caldenius
(1932), Glasser and Jansson (2008), and Davies *et al.* (2020) while the first detailed glacial geomorphological map specific
to the RC and RH valleys was generated by Leger *et al.* (2020). These maps enabled the identification of at least eight
stratigraphically-distinct moraine-outwash complexes deposited by the RC outlet glacier (Fig. 1c). This study focuses on
155 dating results from the three stratigraphically oldest glacial margins: *i.e.* the RC 0 (outermost), RC I and RC II (Fig. 1c)
moraine-outwash complexes. Directly inboard of these margins, the RC outlet glacier deposited another series of at least five
younger moraine complexes (RC III-VII moraines), previously dated to between 26.4 ± 1.4 ka and 19.9 ± 1.1 ka using TCN
exposure dating and Bayesian age modelling (Leger *et al.*, 2021a). The latter moraine belts reflect the local Last Glacial
Maximum (LGM) expansions of the PIS.

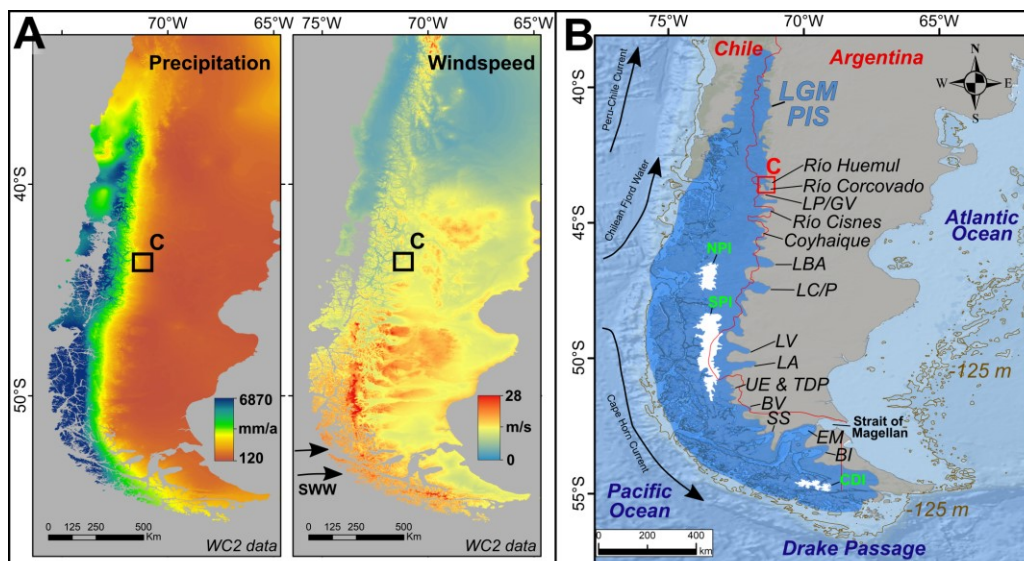
160



165

170

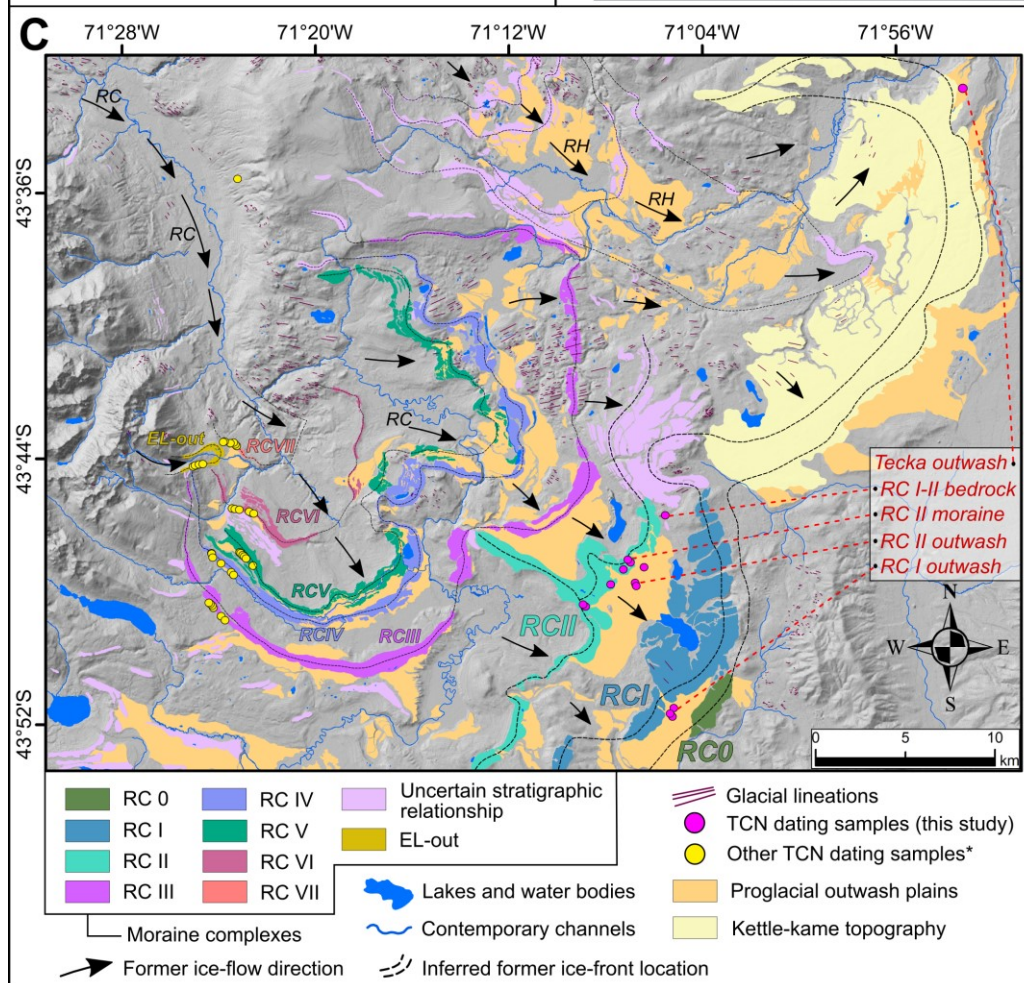
175



180

185

190



195



200 **Figure 1. (A): 1-km² spatial resolution total annual precipitation (mm a⁻¹) and mean annual windspeed (m s⁻¹) land data (1970-2000 mean) from the WorldClim version 2.1 dataset (Fick and Hijmans, 2017) overlaying maps of southernmost South America with location of study area highlighted by black box. (B): Adapted from Leger *et al.* (2020; 2021 a,b): Approximate former extent of the PIS during the LGM, modified from Glasser and Jansson (2008). Locations of major PIS paleo-outlet glaciers are designated: BI: Bahía Inútil, EM: Estrecho de Magallanes, SS: Seno Skyring, BV: Bella Vista, TDP & UE: Torres del Paine & Última Esperanza, LA: Lago Argentino, LV: Lago Viedma, LC/P: Lago Cochrane/Pueyrredón, LBA: Lago Buenos Aires, LP/LGV: Lago Palena/General Vintter. NPI, SPI and CDI stand for North, South, and Cordillera Darwin Patagonian ice fields, respectively. A -125 m (brown-coloured) topographic contour roughly simulating former coastline locations at the LGM is displayed (after Lambeck *et al.*, 2014). Bathymetric data were acquired from the General Bathymetric Chart of the Oceans (GEBCO). (C): Glacial geomorphology of the study area indicating stratigraphic relationship of moraine-outwash complexes preserved, sample site location, and former ice-flow direction.**

205

210 3 Methods

Preliminary identification and mapping of major glacial sediment-landform assemblages studied here was carried out using remotely-sensed imagery and topographic data. These geomorphological interpretations were then ground-checked during a 5-week field season during the 2020 austral summer. Details of the geomorphological mapping methodology and criteria, and the complete map of the study area, are given by Leger *et al.* (2020). To date the RC 0 - II glacier advances, we sampled both outwash surface cobbles and moraine boulders. Specifically, we measured ¹⁰Be in five cobbles from the outermost proglacial outwash surface sampled; here termed the “Tecka outwash”, which we correlate stratigraphically with the RC 0 advance (Fig. 1c). We sampled five and six cobbles respectively from the RC I and RC II outwash terraces, six moraine boulders from the RC II moraine complex, and one ice-moulded bedrock surface located between the RC I and II margins (Figs. 1-3). Additionally, we measured ²⁶Al in five of these 23 samples to determine whether they present simple or complex exposure/burial histories. The chosen moraine boulders are large (90-200 cm high) and rounded to sub-rounded granodiorite and granite erratics embedded in the RC II moraine crest (Fig. 3). The top 2-5 cm of boulder surfaces exhibiting glacial polish were sampled using hammer, chisel and angle grinder.

215

220

225 To date the formation of proglacial outwash plains, quartz-bearing and fluviially-rounded cobbles (4-10 cm diameter; crushed whole) were sampled from well-preserved terraces characterised by low surface gradients (~0.5°-1°), following the procedure established by Hein *et al.* (2009; 2011) (Fig. 2a-d). Surface ventifacts and desert varnish, indicative of prolonged cobble exposure, were considered a required sampling criterion. Sample preparation and cosmogenic isotope ratio measurements were conducted at three different laboratories: the cosmogenic isotope analysis and AMS facilities of the Scottish Universities Environmental Research Centre (SUERC) (East Kilbride, UK), the French National Cosmogenic Nuclides Laboratory (LN2C) and the ASTER AMS facility of the European Centre for Research and Teaching in

230



Environmental Geosciences (CEREGE, Aix-en-Provence, France), and the University of Edinburgh's Cosmogenic Nuclide Laboratory (Edinburgh, UK). Sample details and nuclide concentrations are displayed in Table 1. Details relevant to sample location, photographs, preparation, and wet chemistry are provided in the supplementary materials.

235

^{10}Be and ^{26}Al exposure ages were calculated using the online calculator formerly known as the CRONUS-Earth online calculator version 3 (Balco *et al.*, 2008). Rock density is assumed to be 2.65 g cm^{-3} and elevation flag is STD. For ^{10}Be exposure-age calculations, we used the *NIST_27900* standardisation (equivalent to 07KNSTD within rounding error) and the central Patagonia production rate (Kaplan *et al.*, 2011) obtained and re-calculated from the ICE-D online database (<http://calibration.ice-d.org/>). Details regarding specific AMS standards, nominal $^{10}\text{Be}/^9\text{Be}$ ratios and ^{10}Be half-life employed are included in the supplementary materials. ^{26}Al exposure ages were calculated using the Purdue *Z92-0222* AMS standardisation (equivalent to KNSTD within rounding error) and the default CRONUS-Earth online calculator's global production rate of Borchers *et al.* (2016), as the central Patagonia production rate does not feature $^{26}\text{Al}/^{27}\text{Al}$ measurements. We however consider it reasonable to use both the central Patagonia and global production rates when comparing ^{10}Be and ^{26}Al ages, as their respective ^{10}Be calibrations agree within error, with reported LSDn scaling- fitting parameter values of 0.823 ± 0.067 and 0.846 ± 0.040 , respectively (calibration: ICE-D online database). All exposure ages are displayed in Table 2. Below, we discuss exposure ages calculated using the time-dependent LSDn scaling scheme of Lifton *et al.* (2014) with 1σ analytical uncertainties. Exposure ages are between 6-9% and 0.6-1% older when using the *St* and *Lm* scaling schemes of Lal (1991) and Stone (2000), respectively. The ^{10}Be New Zealand production rate (Putnam *et al.*, 2010), often used for Patagonian TCN exposure-age datasets due to its southern mid-latitude location (44°S), decreases our exposure ages by between 1.7% and 1.5% using LSDn scaling, which is less than 1σ analytical uncertainties (3.5-1.6%).

255

260

265



270

275

280

285

290

295

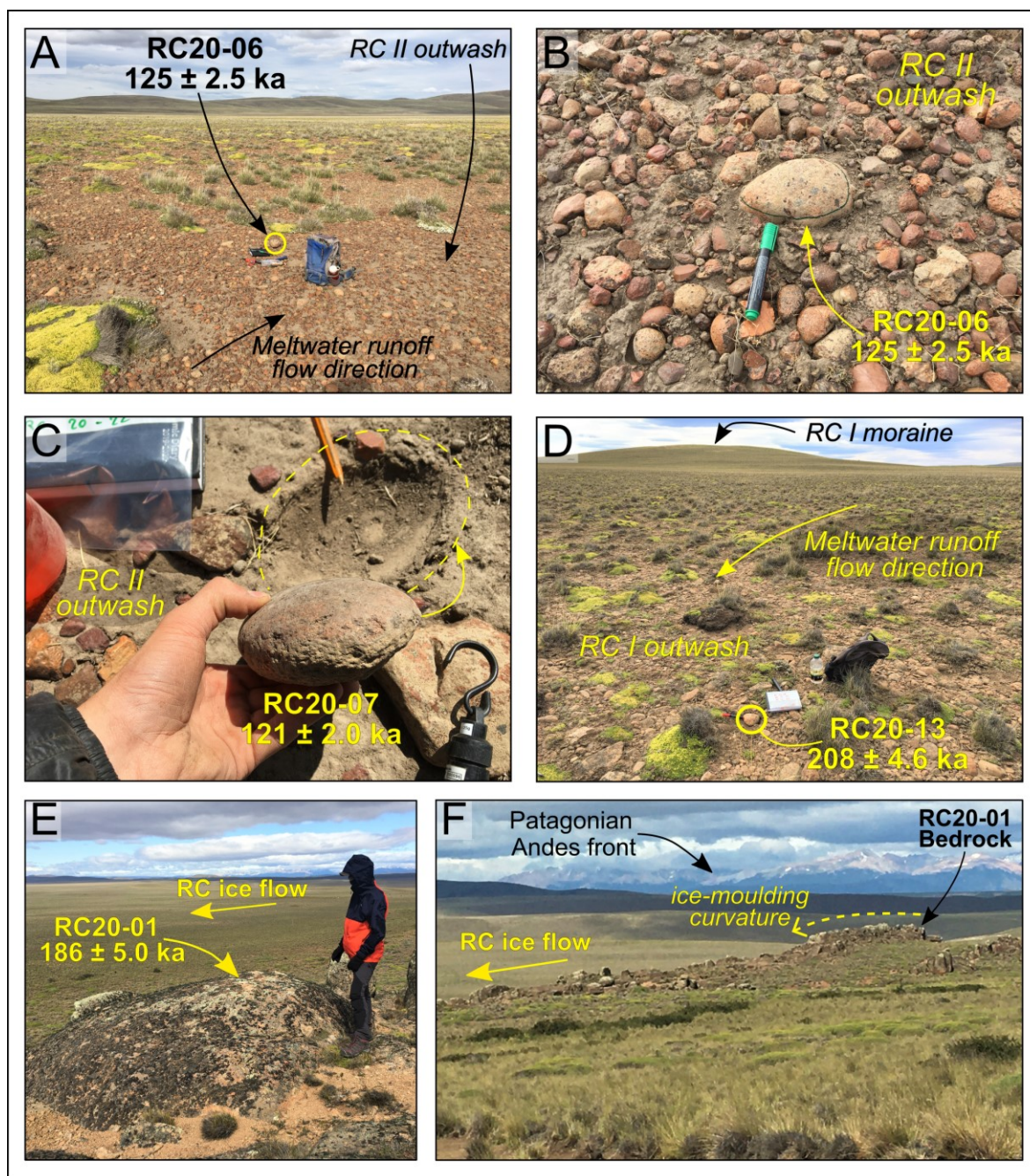


Figure 2. Field photographs of: (A-D) proglacial outwash plains and outwash surface cobbles sampled for TCN exposure dating and; (E, F) the ice-moulded bedrock surface sampled (RC20-01). Ages displayed are ^{10}Be exposure ages $\pm 1\sigma$ analytical uncertainties. Further sample coordinates and characteristics are presented in Table 1.

300

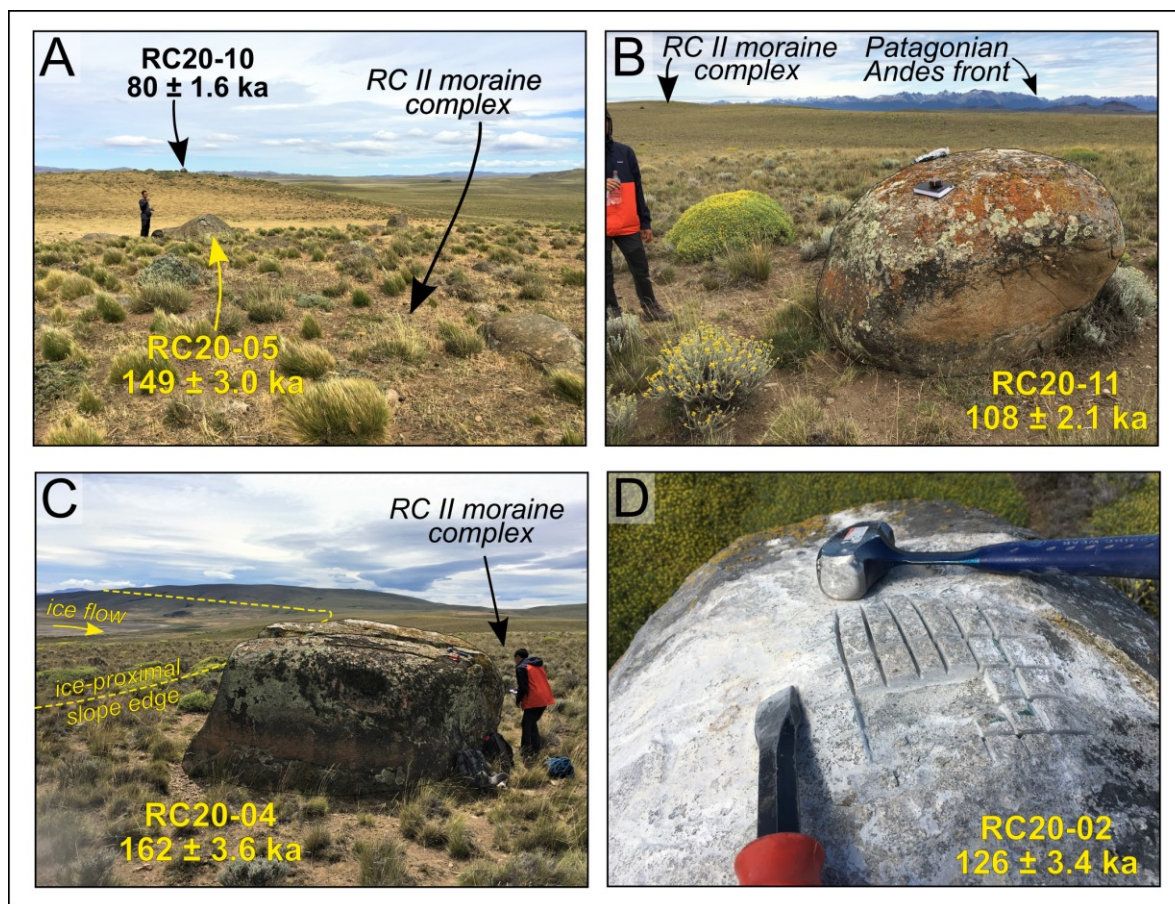


Figure 3. Field photographs of moraine granite and granodiorite boulders sampled for TCN exposure dating. Ages displayed are ^{10}Be exposure ages $\pm 1\sigma$ analytical uncertainties.



4 Results

335 4.1 Geomorphology

In the RC valley, the three most distal preserved moraine complexes (RC 0-II) are morphologically distinct from the younger LGM moraines (RC III-VII). They display greater relief (70-90 m) than the RC III – VII moraines (10-40 m; Leger *et al.*, 2021a), are more subdued, and have broader-crested ridges. The three moraine complexes are 14 km (RC 0), 12 km (RC I) and 5 km (RC II) more distal than the outermost-dated LGM moraine (RC III). The sampled RC II moraine is a ~1 km-wide multi-ridge complex presenting a flat-topped, subdued crest surface elevated up to 45 m above its ice-distal outwash plain. Ice-distal slope gradient is variable but does not exceed 5°, a relatively low grade compared to the slopes of the younger, better preserved LGM moraines which feature slope gradients of 9-19° (Leger *et al.*, 2021a). The RC I moraine complex features slope gradients (>5°) and surface geomorphologies for individual moraine ridges comparable to the RC II moraine belt, but is much wider in places (up to 4.6 km) and exhibits a greater concentration of distinct hummocky ridges and moraines. The subdued moraine geomorphologies characteristic of the RC 0-II margins are suggestive of progressive lateral slope downwasting and moraine surface erosion of fine material post-deposition (Clapperton, 1993; Glasser and Jansson, 2008; Hein *et al.*, 2017). Geomorphological observations thus suggest the RC II and older moraine complexes were deposited significantly prior to the local LGM. In the adjacent RH valley, the outermost glacial margin consists of a ~2 km-wide belt of kettle-kame topography displaying a chaotic hummocks-and-hollows configuration, and was formerly termed the “Tecka drift” (Haller *et al.*, 2003; Leger *et al.*, 2020). The sampled Tecka outwash surface marks the distal limit of this kettle-kame glaciogenic deposit (Fig. 1c). Based on geomorphological mapping and moraine-complex traceability across the RC and RH valleys, the Tecka limit (RH valley) is assumed here to correspond stratigraphically to the RC 0 advance, for which no well-preserved outwash plain surface could be found in the RC valley (Fig. 1c).

355 The outwash surfaces sampled in this study all present long-term preservation properties (Fig. 2). They display low-gradient surfaces (0.5-1°), desert pavements, sparse vegetation cover, and preserved braided palaeo-meltwater channels suggestive of limited surface erosion/deflation (Fig. 2a,d; Leger *et al.*, 2020). These glaciofluvial terraces are composed of sorted and fluviually-rounded sands and gravel deposits. Near the locations of outwash cobble sampling, the outwash surfaces display no detectable signs of post-deposition activation and/or incision by post-glacial hydrology. Where checked, modern soil thickness varied between 0 and 20 cm. This is comparable to observations made further south in the Lago Pueyrredón (47.3°S) and Lago Belgrano (47.5°S) valleys (Hein *et al.*, 2009; Mendelová *et al.*, 2020). At the locations of sampling, these terraces occur adjacent to moraine complexes and mark their distal limits (Fig. 1c), thus enabling the unambiguous stratigraphic association of an outwash deposit with a specific glacial advance.



365

Table 1. TCN exposure dating sample details and nuclide concentrations.

Sample ID	Latitude (DD)	Longitude (DD)	Elevation (m a.s.l.)	Boulder height (m)	Thickness (cm)	Shielding correction	SiO ₂ mass dissolved (g)	Nuclide	Total ⁹ Be or ²⁷ Al mass (mg)	±1σ (mg)	¹⁰ Be/ ⁹ Be or ²⁶ Al/ ²⁷ Al ratio	±1σ ratio	Blank correction	¹⁰ Be (or ²⁶ Al) atoms g ⁻¹ (SiO ₂)	±1σ atoms g ⁻¹ (SiO ₂)	AMS Cathode code	²⁶ Al/ ¹⁰ Be
RH Teeka outwash surface cobbles																	
19RHS09 [†]	-43.55975	-70.88756	828	n/a	9.0	0.99993	21.4250	¹⁰ Be	0.24843	0.0005	2.6145E-12	6.2270E-14	0.27%	2.0207E+06	6.3160E+04	b11920	n/a
19RHS10 [†]	-43.55975	-70.88756	828	n/a	9.0	0.99993	21.4477	¹⁰ Be	0.24980	0.0005	2.4737E-12	6.2290E-14	0.28%	1.9201E+06	6.2059E+04	b11921	n/a
19RHS12 [†]	-43.55975	-70.88756	828	n/a	9.0	0.99993	20.3129	¹⁰ Be	0.24824	0.0005	2.7806E-12	3.5750E-14	0.25%	2.2653E+06	5.4118E+04	b11922	n/a
19RHS13 [†]	-43.55975	-70.88756	828	n/a	10.0	0.99993	20.5896	¹⁰ Be	0.24882	0.0005	2.5549E-12	2.7690E-14	0.28%	2.0579E+06	4.7039E+04	b11923	n/a
19RHS15 [†]	-43.55975	-70.88756	828	n/a	7.5	0.99993	20.6152	¹⁰ Be	0.24833	0.0005	2.3316E-12	2.7170E-14	0.30%	1.8715E+06	4.3560E+04	b11924	n/a
RC I outwash surface cobbles																	
RC20-12 ^Δ	-43.86717	-71.09769	989	n/a	5.0	0.99998	1.9101	¹⁰ Be	0.45617	0.0005	1.3234E-13	4.6198E-15	1.46%	2.0812E+06	7.3876E+04	IIDL	n/a
RC20-13*	-43.86717	-71.09769	989	n/a	4.0	0.99998	19.9300	¹⁰ Be	0.22898	0.0005	2.4409E-12	5.0220E-14	0.82%	1.8577E+06	3.8833E+04	b12115	n/a
RC20-14 ^Δ	-43.87017	-71.10005	993	n/a	9.0	0.99998	3.3260	²⁶ Al	2.54269 ^g	0.1086	4.1836E-12	5.8120E-14	0.16%	1.1893E+07	5.3489E+05	a3380	n/a
RC20-15*	-43.87017	-71.10005	993	n/a	5.0	0.99998	19.6520	¹⁰ Be	0.44301	0.0005	1.9378E-13	5.8904E-15	1.02%	1.7071E+06	5.2498E+04	IIDM	n/a
RC20-16 ^Δ	-43.87132	-71.09883	991	n/a	4.5	0.99998	4.5739	²⁶ Al	2.26658 ^g	0.2380	3.8320E-12	5.8150E-14	0.19%	9.8440E+06	1.0466E+06	a3381	n/a
RC20-16 ^Δ	-43.87132	-71.09883	991	n/a	4.5	0.99998	4.5739	¹⁰ Be	0.44368	0.0005	3.5153E-13	8.3475E-15	0.56%	2.2657E+06	5.4143E+04	IIDK	n/a
RC I/H ice-moulded bedrock surface																	
RC20-01*	-43.77036	-71.10018	1026	n/a	1.5	0.99990	7.3150	¹⁰ Be	0.24010	0.0005	8.1397E-13	1.9970E-14	2.35%	1.7405E+06	4.4314E+04	b12105	n/a
RC20-01*	-43.77036	-71.10018	1026	n/a	1.5	0.99990	7.3150	²⁶ Al	2.13039 ^g	0.0748	1.8242E-12	4.4450E-14	0.43%	1.1803E+07	5.0705E+05	a3375	n/a
RC II outwash surface cobbles																	
RC20-06*	-43.79607	-71.11590	974	n/a	7.0	1.00000	13.9770	¹⁰ Be	0.24171	0.0005	9.5491E-13	1.8140E-14	1.99%	1.0800E+06	2.1289E+04	b12111	n/a
RC20-07*	-43.79607	-71.11590	974	n/a	7.5	1.00000	20.5390	¹⁰ Be	0.24078	0.0005	1.3495E-12	2.1480E-14	1.42%	1.0412E+06	1.7088E+04	b12112	n/a
RC20-19*	-43.80491	-71.12183	976	n/a	6.0	1.00000	19.8810	¹⁰ Be	0.23016	0.0005	1.4072E-12	2.6350E-14	1.42%	1.0724E+06	2.0627E+04	b12119	n/a
RC20-20 ^Δ	-43.80491	-71.12183	976	n/a	4.0	1.00000	4.5249	¹⁰ Be	0.43875	0.0005	2.0274E-13	5.7110E-15	0.99%	1.3006E+06	3.7057E+04	IIDN	n/a
RC20-21 ^Δ	-43.80383	-71.12228	977	n/a	5.5	1.00000	6.6173	¹⁰ Be	0.44192	0.0005	2.8334E-13	7.4642E-15	0.70%	1.2555E+06	3.3338E+04	IIDO	n/a
RC20-22*	-43.80383	-71.12228	977	n/a	4.0	1.00000	20.7920	¹⁰ Be	0.23398	0.0005	1.5691E-12	2.4620E-14	1.25%	1.1643E+06	1.8792E+04	b12120	n/a
RC II moraine boulders																	
RC20-02*	-43.79239	-71.12655	984	1.56	2.0	0.99999	15.0190	¹⁰ Be	0.24273	0.0005	1.0789E-12	2.7230E-14	1.76%	1.1433E+06	2.9631E+04	b12106	n/a
RC20-03*	-43.79345	-71.12502	986	0.86	1.4	0.99999	20.0790	¹⁰ Be	0.24451	0.0005	1.2374E-12	1.7440E-14	1.52%	9.9050E+05	1.4486E+04	b12107	n/a
RC20-04*	-43.79690	-71.13014	983	2.00	2.3	0.99999	19.7420	¹⁰ Be	0.23424	0.0005	1.8605E-12	3.8900E-14	1.05%	1.4586E+06	3.1076E+04	b12108	n/a
RC20-04*	-43.79690	-71.13014	983	2.00	2.3	0.99999	19.7420	²⁶ Al	2.86695 ^g	0.0895	2.8238E-12	4.3000E-14	0.21%	9.1319E+06	3.1778E+05	a3376	n/a
RC20-05*	-43.81415	-71.15841	1020	1.15	2.5	0.99999	20.0200	¹⁰ Be	0.23186	0.0005	1.8099E-12	3.4020E-14	1.10%	1.3845E+06	2.6584E+04	b12109	n/a
RC20-05*	-43.81415	-71.15841	1020	1.15	2.5	0.99999	20.0200	²⁶ Al	2.03553 ^g	0.0661	3.9912E-12	6.4770E-14	0.21%	9.0374E+06	3.2871E+05	a3377	n/a
RC20-10*	-43.81509	-71.15717	1029	1.66	1.7	0.99999	10.5800	¹⁰ Be	0.23772	0.0005	5.1964E-13	9.4730E-15	3.73%	7.4934E+05	1.4825E+04	b12113	n/a
RC20-11*	-43.80433	-71.13924	1002	1.55	1.2	1.00000	19.8670	¹⁰ Be	0.23441	0.0005	1.2858E-12	2.4140E-14	1.53%	9.9741E+05	1.9268E+04	b12114	n/a
Blanks																	
RC20-BL	Δ samples	n/a	n/a	n/a	n/a	n/a	n/a	¹⁰ Be	0.44728	0.0005	1.9671E-15	3.0249E-16	n/a	n/a	n/a	IIDP	n/a
CB190421	* samples	n/a	n/a	n/a	n/a	n/a	n/a	¹⁰ Be	0.22855	0.0005	2.1105E-14	2.6590E-15	n/a	n/a	n/a	b12121-blk	n/a
EUTL9	Y samples	n/a	n/a	n/a	n/a	n/a	n/a	²⁶ Al	2.97988 ^g	0.1120	6.1162E-15	1.7660E-15	n/a	n/a	n/a	a3382	n/a
EUTL9	Y samples	n/a	n/a	n/a	n/a	n/a	n/a	¹⁰ Be	0.24843	0.0005	7.0592E-15	1.5050E-15	n/a	n/a	n/a	b11930	n/a

370

375

380

385

Table footnotes. All cobble samples were crushed whole, without prior cutting. Sample preparation and wet chemistry was conducted at three different laboratories: Y samples: The University of Edinburgh's Cosmogenic Nuclide Laboratory (Edinburgh, UK), * samples: The Scottish Universities Environmental Research Centre (SUERC) (East Kilbride, UK), Δ samples: The French National Cosmogenic Nuclides Laboratory (LN2C) of the European Centre for Research and Teaching in Environmental Geosciences (CEREGE, Aix-en-Provence, France). Nuclide ratios in Y and * samples were measured at the SUERC AMS facility (East Kilbride, UK), while Nuclide ratios in Δ samples were measured at the ASTER AMS facility (CEREGE, Aix-en-Provence, France). SiO₂ is the chemical formula of silica (quartz). # Total ²⁷Al mass from both carrier (²⁷Al concentration: 982 ± 0.1 μg g⁻¹) and sample, determined by ICP-OES. Be Carrier solution used at LN2C has a ⁹Be concentration of 3025 ± 9 μg g⁻¹ while carrier solutions used at SUERC and the University of Edinburgh's Cosmogenic Nuclide Laboratory have ⁹Be concentrations of 849 ± 12 μg g⁻¹ and 1000 μg g⁻¹, respectively. Conversions of isotope ratios to ¹⁰Be and ²⁶Al concentrations were conducted following standard equations, as described by Balco (2006).

390

395



400 4.2 TCN exposure-age chronology

The exposure-age results for the 23 samples are presented in Table 2. Four of the five cobbles sampled on the outermost Tecka/RC 0 outwash surface (Fig. 1c) range from 252.0 ± 6.3 ka to 284.1 ± 7.0 ka and afford a mean ^{10}Be exposure age of 268.7 ± 14.4 ka (arithmetic mean $\pm 1\sigma$ standard deviation). One older age (19RHS12: 311.5 ± 8.1 ka) lies outside the
405 remaining population's 95% (2σ) confidence level and is rejected as a statistical outlier. The remaining exposure-age population is relatively well-clustered given the landform age, but still displays a >1 mean square weighted deviation (MSWD) value of 4.38 ($>k = 2.63$). Such a MSWD value is indicative of greater exposure-age scatter than can be predicted by 1σ analytical uncertainties alone (Jones *et al.*, 2019).

410 The five ^{10}Be ages from the RC I outwash surface cobbles range from 185.0 ± 3.0 ka to 257.4 ± 6.6 ka and afford a mean exposure age of 214.0 ± 29.5 ka. Although the age population presents no obvious statistical or stratigraphical outliers, the exposure ages are poorly clustered, and present a high MSWD value of 33.6 ($>k = 2.41$), indicating significantly more exposure-age scatter than solely predicted by analytical uncertainties. From the ^{26}Al measured in two samples (RC20-13 and RC20-15) from this population, the resulting $^{26}\text{Al}/^{10}\text{Be}$ concentration ratios are 6.4 ± 0.3 and 6.0 ± 0.6 , respectively, and are
415 consistent with a single, continuous exposure history post erosion (Granger and Muzikar, 2001; Balco and Rovey, 2008).

The ice-moulded bedrock surface (RC20-01), located inboard of the RC I moraine, yields a ^{10}Be exposure age of 185.7 ± 5.0 ka, an ^{26}Al exposure age of 181.1 ± 8.5 ka, and an $^{26}\text{Al}/^{10}\text{Be}$ concentration ratio of 6.8 ± 0.3 , which is consistent with continuous exposure post erosion of the surface.

420 The six ^{10}Be ages from the RC II outwash surface cobbles range from 120.6 ± 2.0 ka to 146.6 ± 4.3 ka with a mean exposure age of 131.3 ± 11.1 ka. The age population is tightly clustered considering analytical uncertainties associated with TCN exposure dating of pre-LGC landforms, and thus features no obvious statistical or stratigraphical outliers. However, the population still yields a MSWD value of 11.4 ($>k = 2.26$), diagnostic of some non-analytical exposure-age scatter in the ^{10}Be
425 age distribution.

Three of the six ^{10}Be ages from the RC II moraine boulders range from 125.5 ± 3.4 ka to 161.9 ± 3.6 ka and afford a mean exposure age of 145.3 ± 18.4 ka. Younger ages from the remaining three boulders (RC20-03, 10, 11) plot outside the remaining boulder population's 95% confidence level and the 2σ envelope associated with the youngest RC II outwash
430 cobble (RC20-07). We consider ^{10}Be inheritance an unlikely source of exposure-age scatter compared to the high potential for boulder exhumation causing young outliers. Moreover, the RC II outwash and RC II moraine belt are geomorphologically likely to represent the same glacier expansion event. Hence, these three younger boulder ages were



435 rejected as stratigraphical and statistical outliers (Table 2). The three remaining moraine boulder ages still exhibit a high
MSWD value of 28.7 ($>k = 3.0$), indicating that the remaining dataset displays substantially more exposure-age scatter than
can be predicted solely by analytical uncertainties. The two oldest sampled boulders, RC20-04 (161.9 ± 3.6 ka) and RC20-05
(148.6 ± 3.0 ka), yielded ^{26}Al exposure ages of 143.6 ± 5.4 ka and 137.5 ± 5.4 ka, corresponding to $^{26}\text{Al}/^{10}\text{Be}$ concentration
ratios of 6.3 ± 0.3 and 6.5 ± 0.3 , respectively. Such ratios are consistent with continuous exposure post erosion.

440

445

450

455

460

465



Table 2. TCN exposure ages and summary statistics.

Sample ID	Nuclide	LSDn			St			Lm			Outlier
		Age	Internal	External	Age	Internal	External	Age	Internal	External	
Tecka drift outwash surface cobbles											
19RHS09	¹⁰ Be	276461	9267	25853	299616	10102	28347	278319	9333	26176	
19RHS10	¹⁰ Be	262261	9057	24545	283596	9847	26839	263892	9117	24837	
19RHS12	¹⁰ Be	311517	8053	28598	339128	8829	31545	313965	8121	29001	Yes
19RHS13	¹⁰ Be	284138	6979	25816	308209	7617	28348	286092	7030	26152	
19RHS15	¹⁰ Be	251988	6251	22738	272373	6791	24856	253561	6292	23017	
Mean (n = 5): 277.27 ka; 1σ std: 22.83 ka											
Mean (n = 4): 268.71 ka; 1σ std: 14.37 ka; 1σ internal: 15.99 ka; 1σ internal + PR%: 28.35 ka											
Oldest cobble (n=4): 284.14 ka; 1σ internal: 6.98 ka											
Uncertainty weighted mean (n = 4): 268.06 ka; 1σ std: 13.11 ka											
MSWD: 4.38 > k : 2.63 (n=4); Peak age (n=4): 281.26 ka											
RC I outwash surface cobbles											
RC20-12	¹⁰ Be	236643	8917	22310	258263	9785	24618	240146	9057	22775	
RC20-13	¹⁰ Be	208105	4584	18433	226933	5023	20322	211056	4653	18815	}
	²⁶ Al	191679	9487	20471	203478	10131	25523	189094	9347	21655	
RC20-14	¹⁰ Be	198062	6403	18118	215770	7007	19941	200857	6498	18484	
RC20-15	¹⁰ Be	184989	2957	16053	200289	3214	17559	187105	2993	16340	}
	²⁶ Al	157741	18142	23333	166261	19204	26863	155152	17821	23787	
RC20-16	¹⁰ Be	257360	6563	23302	281123	7213	25764	261214	6668	23806	
Mean (n = 5): 214.03 ka; 1σ std: 29.48 ka; 1σ internal: 13.90 ka; 1σ internal + PR%: 23.27 ka											
Oldest cobble (n=2): 257.36 ka; 1σ internal: 6.56 ka;											
Uncertainty weighted mean (n = 5): 209.46 ka; 1σ std: 25.91 ka											
MSWD: 33.57 > k : 2.41 (n=5); Peak age (n=5): 185.20 ka											
RC I-II ice-moulded bedrock surface											
RC20-01	¹⁰ Be	185674	4954	16596	201425	5395	18184	187977	5018	16904	}
	²⁶ Al	181079	8514	19053	191447	9049	23703	178385	8376	20151	
RC II outwash surface cobbles											
RC20-06	¹⁰ Be	124477	2532	10758	133895	2730	11671	125552	2554	10915	
RC20-07	¹⁰ Be	120592	2040	10323	129458	2195	11177	121543	2057	10467	
RC20-19	¹⁰ Be	122414	2428	10560	131578	2616	11448	123440	2449	10712	
RC20-20	¹⁰ Be	146616	4334	13121	158063	4686	14269	148078	4379	13328	
RC20-21	¹⁰ Be	142948	3935	12689	154172	4256	13805	144388	3976	12891	
RC20-22	¹⁰ Be	130620	2179	11202	140785	2354	12182	131858	2200	11378	
Mean (n = 6): 131.28 ka; 1σ std: 11.05 ka; 1σ internal: 7.45 ka; 1σ internal + PR%: 13.32 ka											
Oldest cobble (n=6): 146.62 ka; 1σ internal: 4.33 ka;											
Uncertainty weighted mean (n = 6): 128.88 ka; 1σ std: 9.03 ka											
MSWD: 11.36 > k : 2.26 (n=6); Peak age (n=6): 121.96 ka											
RC II moraine boulders											
RC20-02	¹⁰ Be	125486	3356	11064	135098	3622	12012	126630	3388	11230	
RC20-03	¹⁰ Be	108441	1630	9217	115730	1742	9917	109171	1641	9335	Yes
RC20-04	¹⁰ Be	161918	3593	14192	174602	3887	15448	163599	3632	14426	}
	²⁶ Al	143604	5367	14309	151277	5676	17887	141129	5268	15174	
RC20-05	¹⁰ Be	148589	2962	12902	160552	3210	14070	150344	2998	13134	}
	²⁶ Al	137464	5353	13743	145113	5673	17185	135316	5264	14587	
RC20-10	¹⁰ Be	79902	1613	6830	84106	1699	7241	80260	1620	6900	Yes
RC20-11	¹⁰ Be	107548	2134	9245	114817	2283	9949	108339	2151	9368	Yes
Mean (n = 6): 121.98 ka; 1σ std: 29.92 ka											
Mean (n = 3): 145.33 ka; 1σ std: 18.43 ka; 1σ internal: 5.74 ka; 1σ internal + PR%: 13.55 ka											
Uncertainty weighted mean (n = 3): 145.12 ka; 1σ std: 14.70 ka											
MSWD: 28.73 > k : 3.0 (n=3); Peak age (n=3): 148.61 ka											

470

475

480

485

490

495

500



505 Table footnotes. ^{10}Be and ^{26}Al exposure ages were calculated using “the online calculator formerly known as the CRONUS-Earth
online calculator version 3” (Balco *et al.*, 2008). Rock density is assumed to be 2.65 g cm^{-3} and elevation flag is STD. All samples
were collected in 2020, thus considered the year of reference for “before present” (BP). ^{10}Be ages reported here are calculated
510 using the central Patagonia production rate (Kaplan *et al.*, 2011) while ^{26}Al ages are here calculated using the global ^{26}Al
production rate of Borchers *et al.* (2016). AMS standardizations employed for calculator input data are NIST_27900 (^{10}Be) and
Purdue Z92-0222 (^{26}Al). Scaling schemes: St is the time-independent version of Lal (1991) and Stone (2000), Lm is the time-
dependent version of Lal (1991) and Stone (2000), and LSDn is the time-dependent scheme of Lifton *et al.* (2014). Ages are
reported with 1σ analytical and external uncertainties, the latter including production rate and scaling uncertainties. Summary
515 statistics were calculated for each dated landform using only ^{10}Be exposure ages and LSDn scaling. This includes arithmetic means
with 1σ standard deviations (std), 1σ propagated (from individual ages) internal uncertainties, and propagated 1σ internal plus
production rate uncertainty (PR%). Summary statistics for sets of outwash surface cobble ages also display the oldest cobble
exposure age; here considered a better minimum-age estimate of outwash deposit formation. Summary statistics also include
uncertainty-weighted means and 1σ standard deviations, MSWDs and Peak ages; calculated using standard equations as described
by Jones *et al.* (2019). Ages in bold are here interpreted as the most appropriate summary ages per landform and are the ones used
throughout the paper for discussion.

520

525

530

535



540 4.3 TCN exposure-age scatter sources

We consider post-depositional shielding of TCN exposure dating samples by vegetation and/or snow to be negligible given the semi-arid and windy conditions (annual 1970-2000 mean wind speed of $\sim 5.3 \text{ m s}^{-1}$; WorldClim 2.1 data; Fick and Hijmans., 2017) that characterise the study site and more generally the Argentinian steppe foreland (Garreaud *et al.*, 2013; 545 Hein *et al.*, 2009; 2017). Modern daily winter (June-August) precipitation is estimated at 2.2 mm near the sampling site (Fick and Hijmans, 2017), which would represent between 20 and 50 cm thick snowfalls given various snow densities. Snow covers of between 75-150 cm thick persisting for four months of the year are typically required to reduce nuclide production by $\sim 5\%$ (snow density range: $0.16\text{-}0.33 \text{ g cm}^{-3}$; Dunai, 2010). Snow accumulation at the study site is thus considered too low to impact exposure ages beyond analytical uncertainties on 10^5 yr timescales. Cosmogenic nuclide inheritance from previous 550 exposure has been shown to be negligible in other eastern Patagonian valleys (*e.g.* Douglass *et al.*, 2007; Hein *et al.*, 2009) and is considered minimal for our samples based on the long ($>80 \text{ km}$) distance separating glacial deposits and source regions. Such transport distance should have enabled efficient glacial erosion of transported clasts. For moraine boulder samples, we expect the sources of exposure-age scatter to originate mainly from rock surface erosion and boulder exhumation through moraine surface deflation and lateral creep (Putkonen and Swanson, 2003; Briner *et al.*, 2005; Hein *et al.*, 2017). 555

For all outwash surface cobbles sampled, total rock-surface erosion is considered negligible due to the fluvially-rounded nature of target samples. We do, however, expect exposure-age scatter to reflect cobble exhumation via a combination of outwash surface deflation (Hein *et al.*, 2009; Darvill *et al.*, 2015) and near surface turbation (*e.g.* cryoturbation) caused by 560 possible local development of soil permafrost during cold intervals (Trombotto, 2008). We thus assume post-depositional disturbance to predominantly cause cobble exhumation and young apparent exposure ages (Phillips *et al.*, 1990; Hein *et al.*, 2011), and thus consider the oldest cobble exposure age a better minimum-age estimate of outwash-plain stabilisation following glacier-front retreat, with the exception of obvious statistical outliers (Table 2, Fig. 4).

565

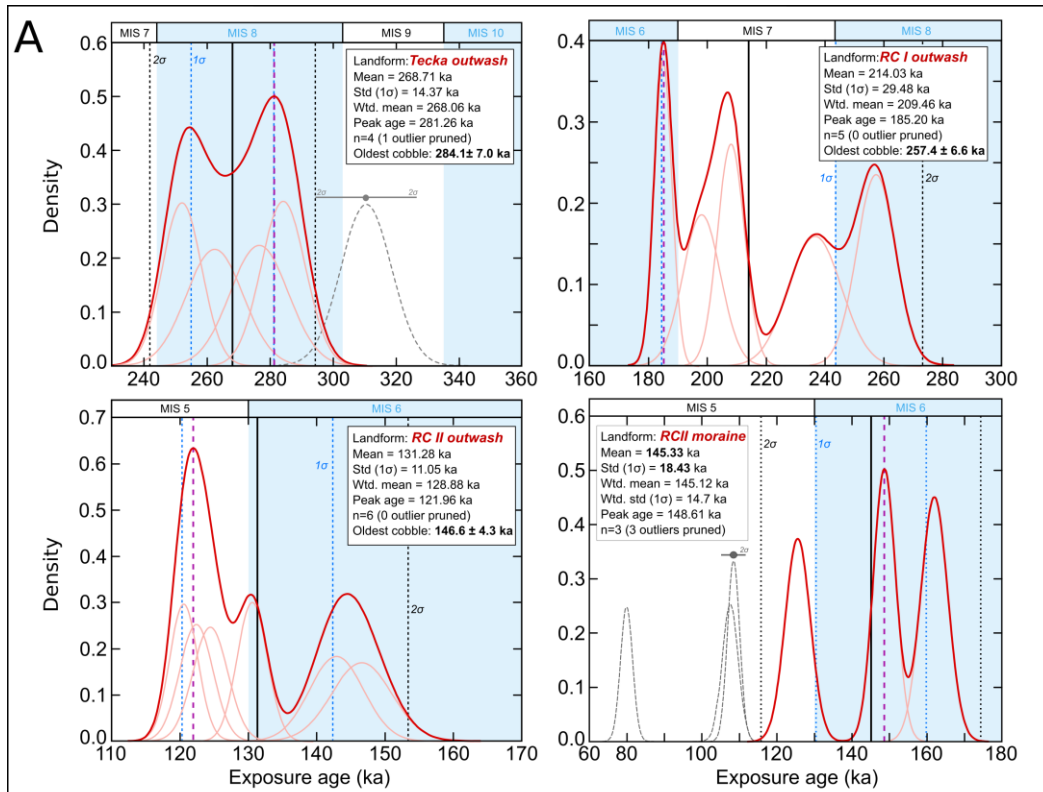
570



575

580

585

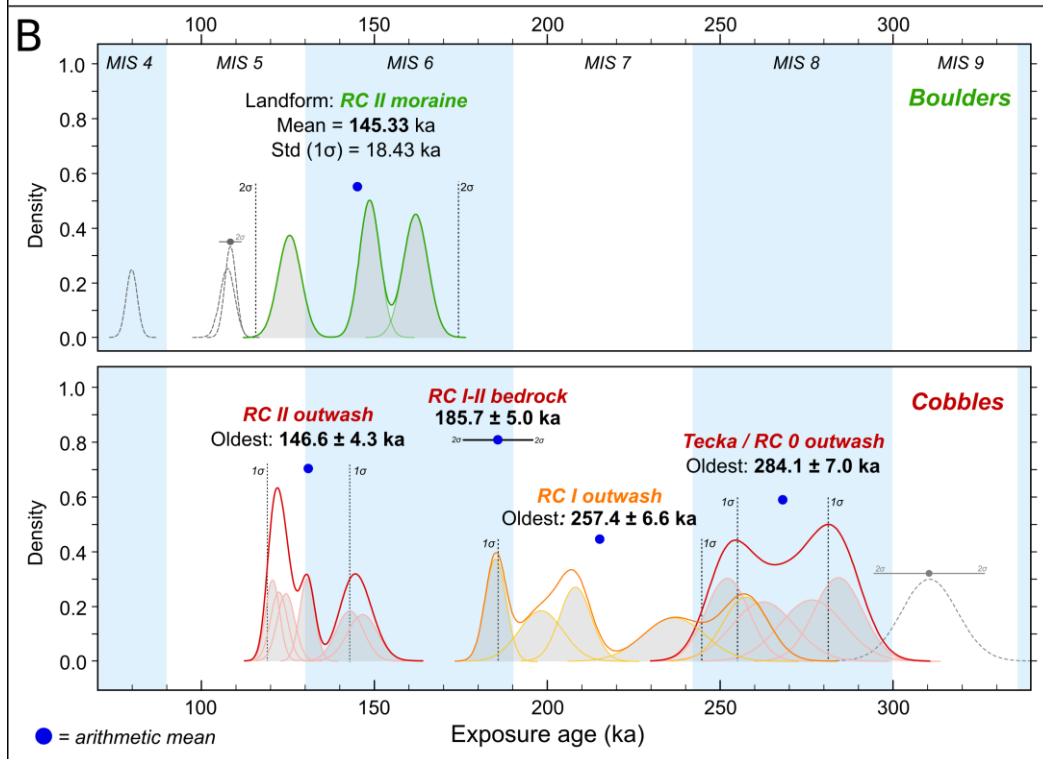


590

595

600

605





610 **Figure 4. (A): Kernel density plots, adapted from IceTEA tools for exposure dating outputs (Jones *et al.*, 2019) and summary statistics for dated landforms. Thick red curve represent the summed probability distribution for the exposure-age population, excluding outliers, while thin red curves depict Gaussian curves for individual samples. Outliers are denoted by grey dashed curves. Vertical black and purple dashed lines denote the population's arithmetic mean and peak ages, respectively. (B): Same kernel density plots as (A) but visualised on single time scale to enable better comparison of different landform ages and relative exposure-age scatter between surface outwash cobble and moraine boulder samples. On both panels, white and blue vertical bands differentiate Marine Isotope Stages (after Lisiecki and Raymo, 2005).**

615 5 Discussion

5.1 TCN exposure age interpretations

5.1.1 The Tecka/RC 0 outwash cobble exposure ages

620 Surface cobbles from the Tecka/RC 0 outwash (Fig. 1c) yield a mean exposure age of 268.7 ± 14.4 ka ($n=4$), excluding one statistical outlier with an age of 311.5 ± 8.1 ka, and display a discernible amount of exposure-age scatter (MSWD: $4.38 > k$). Following the rationale outlined in Sect. 4.3., we consider the outwash's oldest cobble (284.1 ± 7.0 ka) as the closest minimum-age estimate for the RC 0 advance (Figs. 4, 5). The relatively tight cluster of remaining exposure ages ($284 \pm 7 -$
625 252 ± 6 ka) supports this interpretation (Fig. 4).

Here, the outwash terrace sampled features preserved braided meltwater channels that demonstrate minimal outwash surface deflation post deposition. We therefore assess the possible impact of cryoturbation alone on exposure-age underestimation, and estimate broadly the potential magnitude of former cobble exhumation through soil. To do so, we model the constant
630 exhumation of all sampled cobbles (excluding outliers) through a given soil horizon (density: 1.3 g cm^{-3}) and calculate the resulting exposure-age bias caused by cosmic-ray attenuation with depth (Gosse and Phillips, 2001; see supplementary materials). We acknowledge that cobble upfreezing is unlikely to have been continuous and of similar magnitude for all cobbles. We assume that some of this variability is considered by reporting a population mean exposure age post-simulation that matches the original age of the oldest cobble, although this assumption undoubtedly yields uncertainties. Using such
635 simulations, we calculated that a soil thickness of ~ 12 cm would have been required for the Tecka/ RC 0 cobbles to yield a mean ^{10}Be exposure age (283.1 ± 15.0 ka; $+5.7\%$) that approximately matches that of the oldest original surface cobble. This estimated magnitude of cobble upfreezing is plausible given our observations of modern soil thicknesses (0-20 cm) near to the sampling locations. Therefore, despite local semi-arid conditions, cobble exhumation due to cryoturbation through a



640 realistic soil thickness can potentially explain the observed exposure-age scatter (Fig. 5). Such results may also support the hypothesis that outwash surface erosion and deflation was minimal at this location.

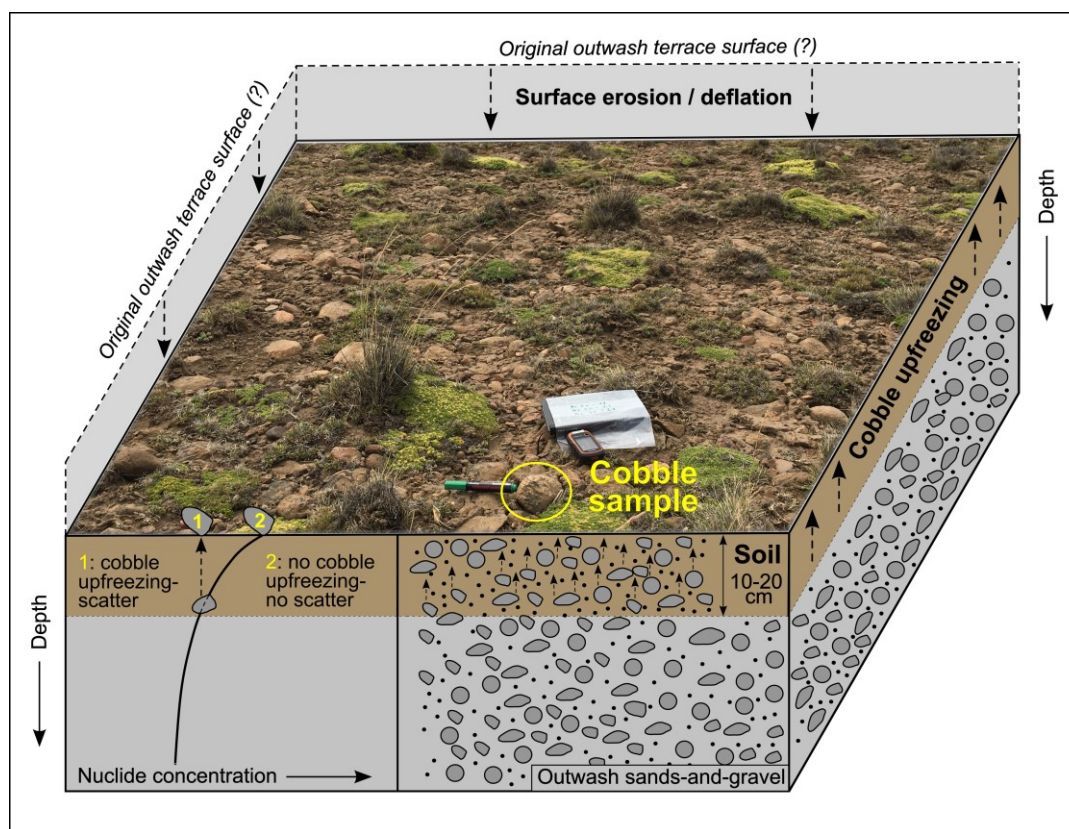
In summary, our interpretations suggest that the exposure ages from the Tecka outwash place the timing of the RC 0 advance at around 290-270 ka, thus during the Marine Isotope Stage (MIS) 8 (300-243 ka; Lisiecki and Raymo, 2005) interval (Figs. 4,6).

645

650

655

660



665 **Figure 5. Illustration of the impact of combined outwash-plain surface deflation and near-surface turbation on exposure-age scatter for outwash surface cobbles sampled. The relationship between depth and nuclide concentration is illustrated by the decay curve (purely schematic) on the bottom left-hand corner of the diagram, which demonstrates that radionuclide production in rock minerals is reduced with depth below surface due to cosmic-ray attenuation. The attenuation effect causes cobbles that have experienced some exhumation post-deposition, due to the effect of upfreezing (dashed vertical arrows; scenario 1), to display exposure-age scatter causing landform deposition age underestimation. Cobbles that remained near the outwash surface since deposition (scenario 2) will display less/no scatter and better estimate the true minimum outwash deposition age. Cobble upfreezing is considered to mainly occur within the soil horizon (brown-coloured) due to the impact of potential permafrost formation. Soil thickness is locally estimated to reach a maximum of ~20 cm. The outwash surface photograph focuses on one of the surface cobble sampled (yellow circle), and enables the assessment of surface cobble density, roundness, size, vegetation type and cover density that are characteristic of outwash plain surfaces sampled within the context of this investigation.**

670

675



5.1.2 The RC I outwash cobbles and timing of the RC I outermost advance

Surface cobbles from the RC I outwash are poorly clustered ($MSWD: 33.6 > k$) and afford a mean exposure age of 214.0 ± 29.5 ka and an oldest cobble age of 257.4 ± 6.6 ka (Table 2, Fig. 4). As previously justified (Sect. 4.3.), we consider the population's oldest cobble (257.4 ± 6.6 ka) as the closest minimum-age estimate for the RC I outwash deposition. Simulations of constant cobble upfreezing through soil (Sect. 5.1.1.) demonstrate that a mean exposure age (257.2 ± 35.3 ka: + 20%) similar to that of the oldest original cobble is obtained when simulating constant exhumation through a ~39 cm-thick soil horizon. Although reasonable, this average soil thickness is greater than modern observations (0-20 cm). For these cobbles, three distinct outwash surface locations were sampled. They display near identical surface morphologies, vegetation cover and apparent modern soil thicknesses (Fig. 2d). It is thus challenging to assess whether spatially variable cryoturbation could have contributed to the observed scatter. This may indicate that, additionally to cobble upfreezing, outwash surface deflation played, in this instance, an important role in causing significant exhumation of certain RC I cobbles post deposition. This hypothesis is supported by the observation that RC I cobble exposure ages display three distinct age groups that correspond with the three different sampling locations (Table 1, SM figure 3). The first group (sample RC20-16) yields an exposure age of 257.4 ± 6.6 ka, while the second (RC20-12 and 13) and third (RC20-14 and 15) groups display mean exposure ages of 222.4 ± 20.2 ka and 191.5 ± 9.3 ka, respectively. We note that the 1σ standard deviations associated with these age groups do not overlap. Thus, it seems plausible that outwash surface deflation was greater at the locations of the second and third sample groups and, combined with clast upfreezing, could therefore explain the substantial exposure-age scatter observed in the ^{10}Be age distribution of the RC I outwash cobbles.

An alternative hypothesis to explain the large RC I exposure-age scatter would be to argue that the RC I outwash could be a composite glaciofluvial deposit formed by meltwater runoff associated with numerous distinct RC outlet-glacier advances. While we commonly expect younger glaciofluvial sedimentation to bury previous deposits, certain cobbles associated with the oldest advances could have been remobilised by either meltwater or ice during younger advances and re-deposited towards the outwash surface. The overlap between the youngest RC I outwash cobble age (185.0 ± 3.0 ka) and the deglacial ^{10}Be age (185.7 ± 5.0 ka) obtained from the ice-moulded bedrock surface sampled directly inboard of the RC I limit could support this hypothesis. Moreover, the RC I moraine belt is a wider (~4 km) complex constituted of more ice-contact hummocks and hummocky ridges suggestive of a greater glaciogenic sediment volume than the RC 0 and RC II moraine complexes (Fig. 6a). This geomorphological distinction could signal that a higher number of individual outlet-glacier advances have reached the RC I margin.

Establishing which of the previous hypotheses are more likely to be valid would require a more detailed chronological and sedimentological analysis through a depth profile of the RC I outwash deposit. However, regardless of which mechanism is



710 responsible for the observed exposure-age scatter, we argue the oldest exposure age from the RC I outwash suggests a separate extensive advance of the RC outlet glacier occurred at around 270-245 ka, thus during the latest stage of the MIS 8 interval (Figs. 4,6).

5.1.3 The RC I-II bedrock surface and timing of innermost RC I advances

715

The sampled ice-moulded bedrock's position and elevation (1026 m *a.s.l.*) suggests it was exposed after deglaciation from the RC I moraine-outwash complex, and prior to the RC II advance (Fig. 1c, 6a). Its ^{10}Be age of 185.7 ± 5.0 ka is thus interpreted as a minimum-age estimate of ice-front retreat following the innermost RC outlet-glacier advance reaching the RC I moraine complex. The older RC I outwash-cobble mean exposure age (214.0 ± 29.5 ka) brings further evidence for this stratigraphic relationship. The $^{26}\text{Al}/^{10}\text{Be}$ ratio (6.8 ± 0.3) from this surface bedrock sample does not indicate a complex exposure-burial history, thus suggesting the RC glacier did not advance beyond and bury the bedrock for any prolonged period (SM Fig. 1). This ratio also demonstrates efficient subglacial erosion of the bedrock surface, which created a fresh surface free of inherited nuclides when last ice-covered.

725 Unlike other samples, we noticed signs of surface erosion on the bedrock outcrop (Fig. 2e). The surface demonstrated a lack of fluvio-glacial polish preservation and showed signs of homogeneous granular disintegration of a depth that proved challenging to quantify in the field. We thus suspect a certain degree of exposure-age underestimation from this bedrock sample. Applying the rock-surface erosion rate of 0.2 mm ka^{-1} estimated for semi-arid central Patagonia (Douglass *et al.*, 2007; Hein *et al.*, 2017) increases its age by 3% to 191.3 ± 5.3 ka, which is within 1σ analytical uncertainty. Subsequently, this minimum deglacial exposure age suggests the youngest outlet-glacier advance to have reached the RC I moraine complex had to occur prior to ~ 190 ka. This interpretation is coherent with RC I outwash cobble exposure ages, and together indicate the RC I complex was most likely deposited prior to the MIS 6 (191-130 ka; Lisiecki and Raymo, 2005) cold interval. Because palaeo-climate proxy records such as Antarctic atmospheric temperature and global SST suggest a return to warmer, near-interglacial conditions between the MIS 7d interstadial (~ 220 -230 ka) and ~ 190 ka (Fig. 8; Parrenin *et al.*, 2013; Shakun *et al.*, 2015), it is likely that the innermost RC I advance occurred during, or prior to the MIS 7d interstadial. In fact, the exposure age of the bedrock surface would date to peak MIS 7d Antarctic cooling (*i.e.* 225 ka, Fig. 8) if a surface erosion rate of 1.07 mm ka^{-1} was applied (LSDn age: 225.1 ± 7.5 ka), which lies within reasonable bounds for rock erosion rates in eastern Patagonia (maximum rate: 1.4 mm ka^{-1} ; Kaplan *et al.*, 2005).

740 To summarise, outwash cobble and bedrock ages suggest that outermost RC I glaciogenic deposits were likely deposited by a MIS 8 glacier advance (~ 270 -245 ka), as portrayed by the oldest outwash cobble age (Figs. 6b,7). On the other hand, the



innermost and youngest outlet-glacier advance to have reached the multi-ridge, 4 km-wide RC I moraine complex (Fig. 1c, 6a) may have been significantly younger, and perhaps occurred during the MIS 7d interstadial. However, the latter part of this interpretation remains unclear, due to the lack of chronological data for the innermost RC I deposits combined with the analytical uncertainties and the large scatter displayed by outwash cobble exposure ages from this margin. More
745 chronological constraints are thus required to test this hypothesis.

5.1.4 The RC II outwash cobble and moraine boulder exposure ages

750

As for the older RC I and Tecka outwash cobble samples, we argue the observed scatter (MSWD: 11.4 $>k$) in the RC II outwash cobbles exposure ages (mean: 131.3 ± 11.1 ka) likely originates from cobble exhumation and minor outwash-surface deflation (Fig. 5). This interpretation is reinforced by cobble ages displaying a younger mean age and a tighter cluster than moraine boulders from the stratigraphically -equivalent glacial margin (RC II; Table 2, Fig. 4). Consequently,
755 the oldest surface cobble (146.7 ± 4.3 ka) is deemed a better minimum-age estimate for the RC II glacial advance. We find that a mean exposure age (145.5 ± 12.6 ka: + 11%) similar to that of the oldest cobble can be obtained when simulating constant exhumation of all cobbles (see Sect. 5.1.1.) through a 24 cm-thick soil horizon. This estimate, although highly uncertain, is consistent with modern soil thickness observations near sampling locations (0-20 cm). This simulation suggests that, despite local semi-arid conditions, cobble upfreezing through a realistic soil thickness can cause the observed exposure-
760 age scatter leading to the age underestimation of outwash plain formation. In summary, the RC II outwash cobble ages seem to suggest a minimum-age estimate of ~ 145 ka. Therefore, we argue the RC II limit reflects an extensive expansion of the local PIS outlet glacier occurring towards the latest stage of the MIS 6 cold interval (Figs. 4,6,7).

Following outlier removal ($n = 3$), the RC II moraine boulder mean exposure age ($n = 3$; 145.3 ± 18.4 ka) overlaps the RC II mean outwash cobble age within 1σ analytical uncertainties. The boulder population also displays two ages that are consistent with the set of outwash cobbles (125.5 ± 3.4 ka and 148.6 ± 3.0 ka). These results support our stratigraphic interpretation that these two landforms were deposited by the same outlet-glacier advance. Because we sampled rounded boulders and specifically targeted raised rock fragments presenting fluvioglacial polish, we here consider boulder surface erosion to be negligible, in contrast to the sampled ice-moulded bedrock surface, where granular disintegration was
770 ubiquitous. The population's oldest boulder (RC20-04: 161.9 ± 3.6 ka) displays a ~ 15 ka older exposure age than the oldest RC II outwash surface cobble. Cosmogenic nuclide inheritance from pre-glacial-transport exposure is considered unlikely given the >80 km distance to source region and the sub-rounded morphology of the boulders sampled indicative of subglacial clast erosion (Fig. 3b,c). We instead propose this older boulder may reflect at least one earlier glacial advance to the same terminal position, or may have been re-deposited during the RC II advance following exposure during previous



775 glacier advances reaching proximal inboard ice-front positions. The $^{26}\text{Al}/^{10}\text{Be}$ concentration ratio from this sample (6.3 ± 0.3) does not suggest a prolonged period of boulder burial (SM Fig. 1). We therefore hypothesise previous PIS advances might have locally occurred during earlier MIS 6 cold intervals (e.g. MIS 6c,e), while the youngest penultimate MIS 6 glacial maximum is more accurately dated by the RC II surface outwash cobbles, as the glaciofluvial terraces likely remained active until the end of the glaciation.

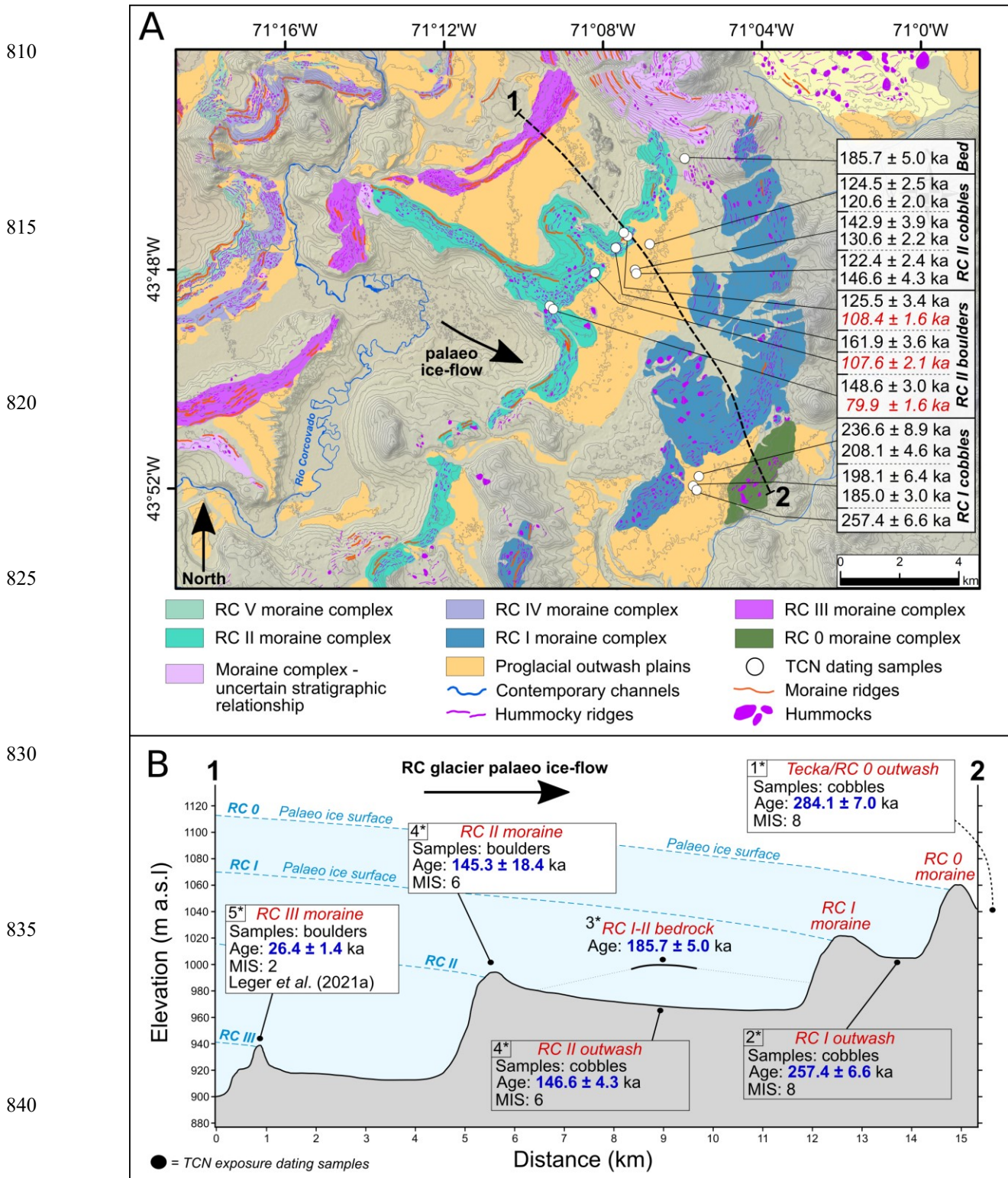
780

Overall, our results from the RC II limit ($n = 12$ ages) indicate that outwash surface cobble ages display less post-depositional scatter than moraine boulder ages, with MSWD values of ~ 11 vs ~ 30 , respectively. This comparison thus agrees with results of Hein *et al.* (2009, 2017) suggesting that well-rounded cobbles sampled from the surface of former proglacial outwash plains are better-suited to numerically date pre-LGC glaciations in semi-arid, undisturbed environments such as the Argentinian steppe of Patagonia. However, even if semi-arid conditions usually limit soil thickness to <20 cm on outwash plains of the Argentinian steppe, our simulations show that potential cobble exhumation due to cryoturbation alone can cause meaningful landform-age underestimations for pre-LGC glacial deposits. This source of post-depositional exposure-age scatter is thus important to consider when interpreting outwash surface cobble exposure ages. Another advantage of targeting outwash cobbles is their abundance in formerly active glaciofluvial environments, while moraine boulders on pre-LGC margins are often sparse and where found, are highly eroded. This enables rigorous selection of cobbles that are most suitable to TCN exposure dating. On the other hand, obtaining exposure ages from both moraine boulders and outwash cobbles can provide additional insight on former glacier activity that may not be evident without the combined approach.

795

800

805





845 **Figure 6. (A):** Glacial geomorphological map focused on the RC 0 - RC II moraine-outwash sequence around the location of TCN
exposure dating samples, highlighted by white dots (with the exception of Tecka/RC 0 outwash samples (Fig. 1c)). Exposure ages
displayed are ^{10}Be ages $\pm 1\sigma$ analytical uncertainties, calibrated with LSDn scaling and central Patagonia production rate (Kapan
et al., 2011). Ages in red were interpreted as outliers. “Bed” stands for “bedrock” and depicts the RC I – RC II ice moulded
bedrock surface sampled. Elevation data is provided by the 30-m resolution DEM from the ALOS World 3D missions (AW3D30,
version 2.2; JAXA; <https://www.Eorc.jaxa.jp/ALOS/en/aw3d30/>) with a shaded relief background and elevation contour lines at
15-m intervals. (B): Simplified and smoothed elevation profile graph (DEM data: AW3D30) drawn along the black line denoted in
850 panel (A), with TCN exposure dating results (^{10}Be) from the RC 0 - III moraine-outwash dataset after interpretation of the best
minimum-age estimate for each dated landform. Palaeo-ice surface elevation and slope gradients are hypothetical and purely
schematic. *: Stratigraphic order of events (1: oldest, 5: youngest).

855

5.2 Comparisons with palaeo-climate and global cryosphere contexts

5.2.1 The MIS 8 glaciations

860

Our chronology suggests that two of the most extensive PIS advances preserved at the study site (RC 0 and RC I outermost)
occurred during MIS 8, at around 290-270 ka, and 270-245 ka, respectively (Figs. 6,7). These expansion events are coeval,
within dating uncertainties, with glacial advances recorded by the two largest outlet glaciers of the former PIS in central
Patagonia. There, the penultimate glacial advance in both the Lago Buenos Aires valley (46.5°S; Hein *et al.*, 2017; Fig. 1)
865 and the Lago Pueyrredón valley (47.5°S; Hein *et al.*, 2009), are thought to have occurred during MIS 8. Altogether, these
three pre-LGC Patagonian TCN chronologies indicate that the MIS 8 glacial events were some of the PIS’s most extensive
Pleistocene glaciations. These advances likely affected the former PIS across a large latitudinal range, as they can now be
traced across multiple valleys from central to northern Patagonia. The geographical ubiquity of these events is diagnostic of
a strong climatic forcing, while their timing coincides with some of the lowest middle Pleistocene δD values recorded over
870 Antarctica at around 280-270 ka, associated with maximum MIS 8 Antarctic cooling of -8.5°C relative to pre-industrial
modern temperatures (Parrenin *et al.*, 2013; Fig. 8). The RC 0 advance may also be coeval with a severe peak in dust flux
recorded in the EDC Antarctic ice core at ~ 270 ka (Lambert *et al.*, 2008; Fig. 8). Isotopic composition analyses have
demonstrated that Antarctic ice-core dust concentrations are positively correlated to outwash-plain activity in southern
Patagonia, and thus may directly reflect PIS outlet-glacier expansion events (Sugden *et al.*, 2009; Koffman *et al.*, 2021).

875

During MIS 8, Northern Hemisphere (NH) mid-latitude summer insolation intensity reached two distinct minima at 280 ka
and 255 ka (Berger and Loutre, 1991; Fig. 8). These troughs are synchronous with peaks in the SH mid-latitude seasonality



curve indicative of colder winters and warmer summers in Patagonia at those times (Darvill *et al.*, 2016). Importantly, the signal of NH mid-latitude summer insolation intensity also mirrors orbitally-controlled SH seasonal duration (Denton *et al.*, 2021). Hence, Patagonia was experiencing longer, colder winters and shorter, warmer summers around 280 ka and 255 ka. In contrast, SH mid-latitude summer insolation intensity reached maximum values at 280 ka and 255 ka, but minimum values at 292 ka and 268 ka, which are within exposure-age scatter and analytical uncertainties associated with dating of the RC 0 and outermost RC I advances (this study), and of the MIS 8 advances of the Lago Buenos Aires and Lago Pueyrredón outlet glaciers also (Hein *et al.*, 2009; 2017). Therefore, due to current TCN exposure dating uncertainties, it remains a challenge to determine whether the MIS 8 Patagonian glaciation was coeval with a SH, or a NH mid-latitude summer insolation intensity minimum. However, more accurate dating of younger PIS outlet-glacier advances occurring during the global LGM (MIS 2; *e.g.* Peltier *et al.*, 2021), including the RC outlet glacier (RC III-VII; Leger *et al.*, 2021a), has shown that these later SH glacier advances, and also SSTs and Antarctic atmospheric temperature depressions, were anti-phased with SH summer insolation intensity, and were instead coeval with high SH seasonality and winter duration. Consequently, it is plausible that the PIS advanced at ~280 ka (RC 0) and ~255 ka (RC I), when SH summer insolation intensity was high, but when SH winters were cold and long. The proposed timing for the RC 0 advance is consistent with other SH palaeo-climate proxy records which suggest that peak MIS 8 cooling occurred relatively early during the glacial cycle (*i.e.* 280-270 ka; Fig. 8), in contrast with the later MIS 6 and MIS 5d to MIS 2 glaciations, which are characterised by maximum global cooling occurring just prior to sudden glacial terminations (Hughes *et al.*, 2020).

Paradoxically, MIS 8 displays a relatively weak global cooling signal in several records such as benthic $\delta^{18}\text{O}$ (Hughes *et al.*, 2020), and is thought to have been characterised by the lowest sea-level depression relative to other middle Pleistocene 100 ka glacial intervals (-93 m; Spratt and Lisiecki, 2016). Moreover, glacial terrestrial records from different regions demonstrate contrasting ice-sheet and glacier behaviours during MIS 8. Indeed, although stratigraphic evidence for MIS 8 glaciations is often elusive, some has been reported for the Fennoscandian and British-Irish ice sheets (Beets *et al.*, 2005; Davies *et al.*, 2012; White *et al.*, 2010; 2017), former ice sheets and glaciers overprinting Poland (Krznanian glaciations; Lindner and Marks; 1999), Siberia and Russia (Astakhov *et al.*, 2011; 2016), Central and southern Europe (*e.g.* Preusser *et al.*, 2011), and the West Coast Range of Tasmania (Colhoun and Barrows, 2011; Kiernan *et al.*, 2010). In North America, chronological constraints for stratigraphic evidence of pre-MIS 6 glacial deposits are, in most cases, too imprecise to determine the marine isotope stage to which they relate (Hughes *et al.*, 2020). The review by Hughes *et al.* (2020) concludes that robust chronological evidence of MIS 8 glaciations is rare, and, where it is found, is often characterised by margins located inboard of MIS 6 limits. In general, direct chronological evidence of MIS 8 glaciations more extensive than MIS 6-2 advances has only been found in Russia (east of the Urals; Astakhov *et al.*, 2016) and Patagonia. Therefore, the extensive MIS 8 glaciation of Patagonia implies a strong regional cooling signal (Hein *et al.*, 2017).

910

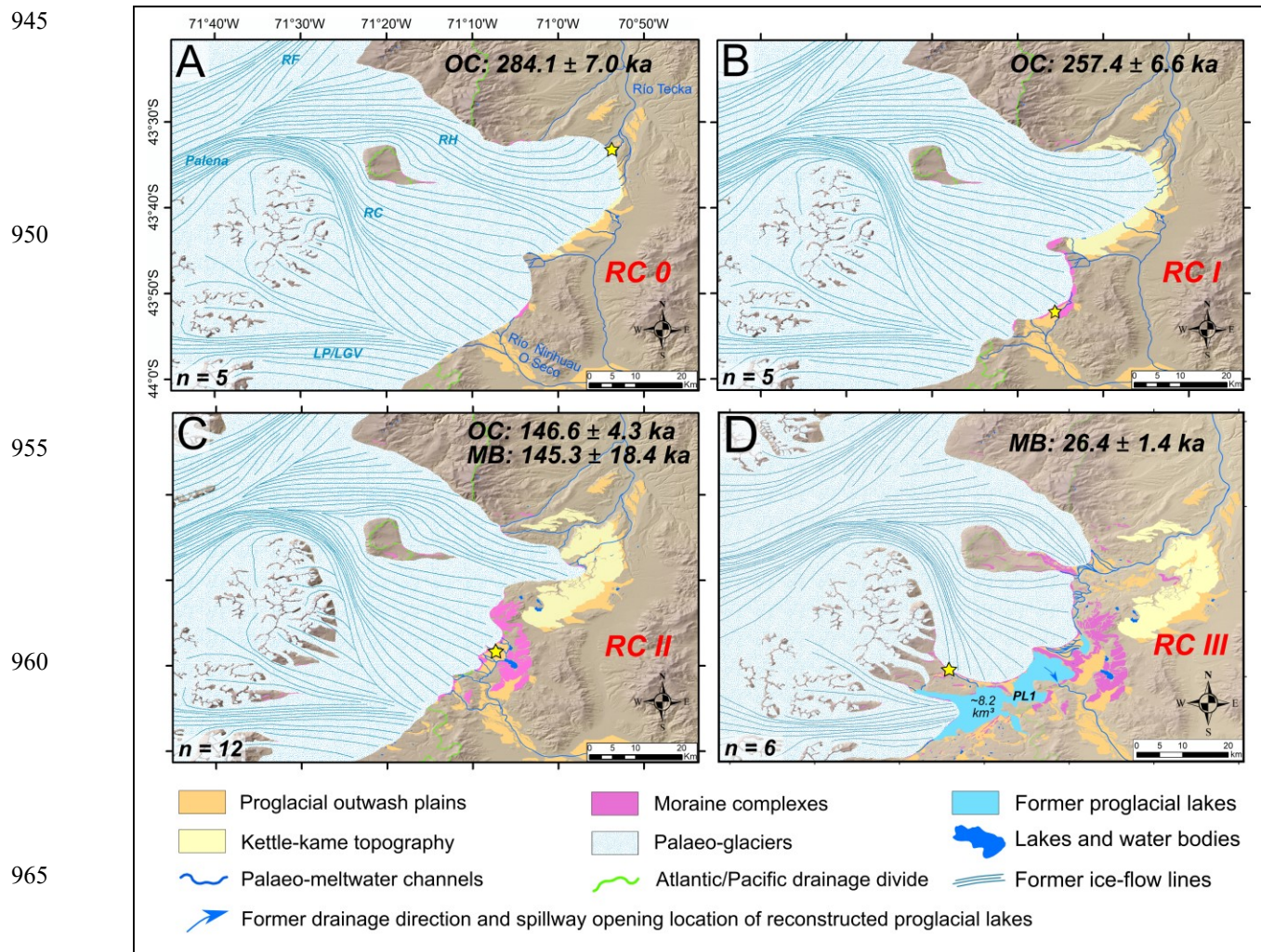


915 It has been noted in previous work that the major eastern Patagonian valleys, including the RC valley (Figs. 6,7), feature records of progressively decreasing glacier extents as the glacier advances get younger (Singer *et al.*, 2004; Kaplan *et al.*, 2009; Cogež *et al.*, 2018). This pattern may not be entirely climate-related. Instead, it might be caused by a combination of long-term erosion of the accumulation area and focused subglacial erosion along former glacial valleys that resulted in glacial overdeepening (Kaplan *et al.*, 2009). During Quaternary glacial cycles, selective subglacial erosion, shown to be most effective along the flowlines of warm-based PIS outlet glaciers and near the centre of the ice sheet where ice was thickest (Clapperton, 1983), has caused rapid and zonally asymmetric overdeepening of main Patagonian valleys (Rabassa and Clapperton, 1990). In the past ~1.2 Ma, this erosive process has been estimated to cause >1000 m of bedrock elevation lowering in certain Patagonian valleys (Singer *et al.*, 2004). Kaplan *et al.* (2009) argued that such overdeepening would likely have overcome the effects of tectonic- and glacial isostatic adjustment-related uplift. For a given location and identical climate forcing, erosion-driven bed lowering may have led to progressively more negative glacier mass balances during each major PIS expansion event, causing less extensive glacier advances with time. Moreover, if more effective towards the former ice divide, subglacial erosion would also have increased retrograde basal slope gradients and thus augmented basal shear stress during subsequent glacier advances. These processes could therefore partly explain the observed pattern of decreasing outlet-glacier extent through time in eastern Patagonia (Fig. 6). Consequently, although the geographically widespread MIS 8 advances of the PIS were most likely the result of strong climate forcing, their outboard positions relative to MIS 6-2 deposits do not necessarily indicate colder regional conditions during MIS 8 than during the younger advances.

930

935

940



945
 950
 955
 960
 965
 970
 975
 980

Figure 7. Palaeo-glacial reconstructions for the RC, RH, RF and Lago Palena/General Vintter (LP/LGV) valleys, for each advances/stillstands and deglacial events interpreted in this investigation (A–C). Panel D displays the ice extent associated with the RC III moraine complex, described in detail in companion publication (Leger *et al.*, 2021a). The latter reconstruction includes the formation of glaciolacustrine phase one (here termed PL1; Leger *et al.*, 2021a). Ice-sheet and mountain glacier models were digitised manually in ArcGIS. Apart from when delineated by confidently-mapped moraine limits (e.g. the RC, RH and LP/LGV moraine sequences), the geographical location of ice margins are inferred from topography. Topographic data is from the AW3D30 DEM. “OC” and “MB” denote the type of rock samples used for TCN exposure dating of the represented event, and stand for “outwash cobbles”, and “moraine boulders”, respectively. Yellow stars indicate the approximate sample locations for TCN exposure dating of each represented event, while each panel features the number of ^{10}Be exposure ages produced ($n = x$) on the bottom left-hand corner (this excludes ^{26}Al ages). There are no previously published glacier chronologies in the RH, RF and LP/LGV valleys. Relative ice extents in those neighbouring valleys are thus inferred from our RC chronology and cross-valley comparisons of moraine set numbers, preservation and morphostratigraphy. Hence, these inferences yield some uncertainties. Proglacial lake volume estimates were computed from DEM data (AW3D30).



5.2.2 The MIS 7 glaciation

985 Our chronology provides inceptive evidence that the innermost and youngest advance to have reached the RC I moraine
complex may have occurred during MIS 7 (243-191 ka; Lisiecki and Raymo, 2005). Although the resolution of our
chronology is not sufficient to assert the following with confidence, we argue that this potential event might relate to
interstadial MIS 7d (~235-225 ka), described in detail by Ruddiman and McIntyre (1982, p1273) as an event that “bisected
990 *interglacial*” isotopic stage 7, lasted no more than 23,000 yr from inception to end, and resulted in a very large ice-volume
build-up and a full-glacial climatic response of the North Atlantic Ocean”. Direct terrestrial evidence and robust dating of
this event are currently non-existent in the southern mid-latitudes, and hence more empirical data from several locations are
required to assess the geographical ubiquity of this glacial expansion event.

During the relatively brief MIS 7d interstadial, global atmospheric CO_2 concentrations are estimated to have diminished by
995 ~75 ppm (Bereiter *et al.*, 2015), and the atmospheric temperature depression over Antarctica was of similar magnitude to that
recorded during the MIS 8 and MIS 6 stadials (Fig. 8). These records indicate that a 20 ka-long Antarctic atmospheric
cooling phase, with a peak cooling of approximately $-7.5^\circ C$ relative to pre-industrial modern temperatures, occurred at ~223
ka, 7 ka after NH mid-latitude summer insolation intensity reached the lowest values of the past 1 Ma, at 230 ka (Fig. 8).
Therefore, while interstadial MIS 7d was relatively short-lived, it was characterised by record-high winter duration and a
1000 peak in local seasonality (colder winters and warmer summers) at the SH mid-latitudes. Antarctic dust concentration records
also indicate a significant maximum at 225-220 ka (Lambert *et al.*, 2008; 2012). This implies the MIS 7d interstadial was
likely associated with an expansion of the PIS inducing outwash-plain activity in southern Patagonia (Sugden *et al.*, 2009).

1005 5.2.3 The penultimate MIS 6 glaciation

Our interpretation of TCN exposure ages from the penultimate RC II margin suggests that a major expansion of the PIS
occurred during MIS 6, and towards the latter part of the glacial interval, at around 140-150 ka (Figs. 4,6,7). Our chronology
suggests that maximum PIS expansion occurred just prior to the rapid global warming leading to MIS 5e, one of the warmer
1010 middle-to-late Pleistocene interglacial periods (Fig. 8). This is consistent with global sea-level reconstructions suggesting
that the second greatest global ice volume of the past 800 ka, associated with a sea-level minimum of -125 m, was reached
towards the end of MIS 6, at ~140 – 135 ka (Spratt and Lisiecki, 2016). At that time, mean atmospheric temperatures over
Antarctica are estimated to have reached their second lowest values of the past 800 ka ($-9.3^\circ C$ relative to pre-industrial
period; Fig. 8). Global cooling during MIS 6 was more persistent than during other middle Pleistocene glacial cycles. Indeed,



1015 this cycle is associated with four major minima in Antarctic atmospheric temperatures spread over ~50 ka, and occurring at
around ~185, ~165, ~155 and ~140 ka (Parrenin *et al.*, 2013; Fig. 8). As observed for the MIS 8 interval, these peaks in
atmospheric cooling occurred a few ka after NH summer insolation intensity minima, associated with SH seasonality and
winter duration maxima. Global SSTs and atmospheric CO_2 concentrations remained consistently low for the same 50 ka
time-window, between ~190 and ~140 ka (Bereiter *et al.*, 2015; Shakun *et al.*, 2015). The persistence of the cold phase
1020 throughout MIS 6 may have facilitated multiple expansions of the PIS at this time. In our ^{10}Be chronology, this may be
reflected by the potential recycling and re-deposition of one RC II moraine boulder sample, yielding a ^{10}Be exposure ages of
 162 ± 4 ka, during the younger penultimate advance dated by the RC II outwash cobbles (~130-140 ka).

Evidence for several distinct MIS 6 glaciations has been reported from other regions of the world. For the European Ice
1025 Sheet, for instance, stratigraphic investigations have led to the dating, and naming, of two glaciations within MIS 6,
respectively the Late Saalian Drenthe glaciation at 175-155 ka, and the Warthe Stadial between 150 ka and 135 ka
(Toucanne *et al.*, 2009; Margari *et al.*, 2014). More generally, MIS 6 glacial deposits are ubiquitous near former glacial
margins and are documented by a wider body of evidence than other pre-LGC glaciations (*e.g.* Putnam *et al.*, 2013; Kiernan
et al., 2014; Evans *et al.*, 2019; Fernandes *et al.*, 2021), suggesting that the greatest global ice volume of the middle
1030 Pleistocene was likely reached during that interval (Hughes *et al.*, 2020). In Patagonia, however, our chronology is amongst
the first published datasets, along with one other ongoing investigation (abstract: Peltier *et al.*, 2017), offering direct and
robust dating of a MIS 6 glacial expansion event. Indeed, the well-studied Lago Pueyrredón and Lago Buenos Aires pre-
LGC moraine-outwash records do not provide clear chronological evidence for MIS 6 advances (Hein *et al.*, 2009; 2017).
However, this may just imply that the MIS 2 advances of the Lago Pueyrredón and Lago Buenos Aires outlet glaciers were
1035 more extensive than any MIS 6 glacial events. Therefore, as for the MIS 8 glaciation, MIS 6 expansions of outlet glaciers
may have been ubiquitous through the former PIS. However, the current lack of robust pre-LGC glacier chronologies in
Patagonia prevents this hypothesis from being tested adequately.

1040

1045



5.2.4 Synthesis: The timing of Patagonian glaciations

1050

Along with companion publications focusing on the LGC (Leger *et al.*, 2020; 2021a), our findings illustrate that the preserved sequence of moraine-outwash complexes in the RC valley system records a minimum of four major PIS expansion events occurring during MIS 8, 6, and 2; and possibly also during MIS 7. In Antarctic atmospheric paleo-temperature proxy records, global SST records, and global atmospheric CO_2 records, the strongest minima between today and 330 ka are all recorded by the RC moraine-outwash complexes, with the exception of the 70-60 ka (MIS 4) cold interval, for which no preserved moraine-outwash complex could be found at the study site. However, we note that a major advance of the PIS near this time did occur on the western side of the Andes at 42°S (García *et al.*, 2021; Gómez *et al.*, 2022). There, García *et al.* (2021) dated glacial sediments on the Isle of Chiloe to 57.8 ± 4.7 ka, or early MIS 3, with a somewhat smaller advance occurring during MIS 2 at 26.0 ± 2.9 ka. The lack of a corresponding MIS 3/4 moraine east of the mountains suggests that the PIS behaved asynchronously between its western and eastern margins at this time. In southeastern Patagonia, more-extensive-than MIS 2 advances were also dated to MIS 4 and 3 using TCN exposure dating (*e.g.* Darvill *et al.*, 2016; García *et al.*, 2018; Peltier *et al.*, 2021). We argue that while the RC outlet glacier most likely advanced during the MIS 4 and 3 cooling events, these intervals were relatively short-lived, impeding the PIS from becoming locally thick enough to allow the RC outlet glacier to advance along its retrograde bed slope and generate an extensive advance. Very likely, in addition, all glaciogenic deposits associated with MIS 3/4 advances may have been eroded during the younger MIS 2 advances. This may suggest that steady cooling over periods >15-20 ka is an important pre-requisite for northeastern PIS outlet glaciers to reach a mass balance positive enough to enable highly extensive advances.

1055

1060

1065

1070

1075

1080



1085

1090

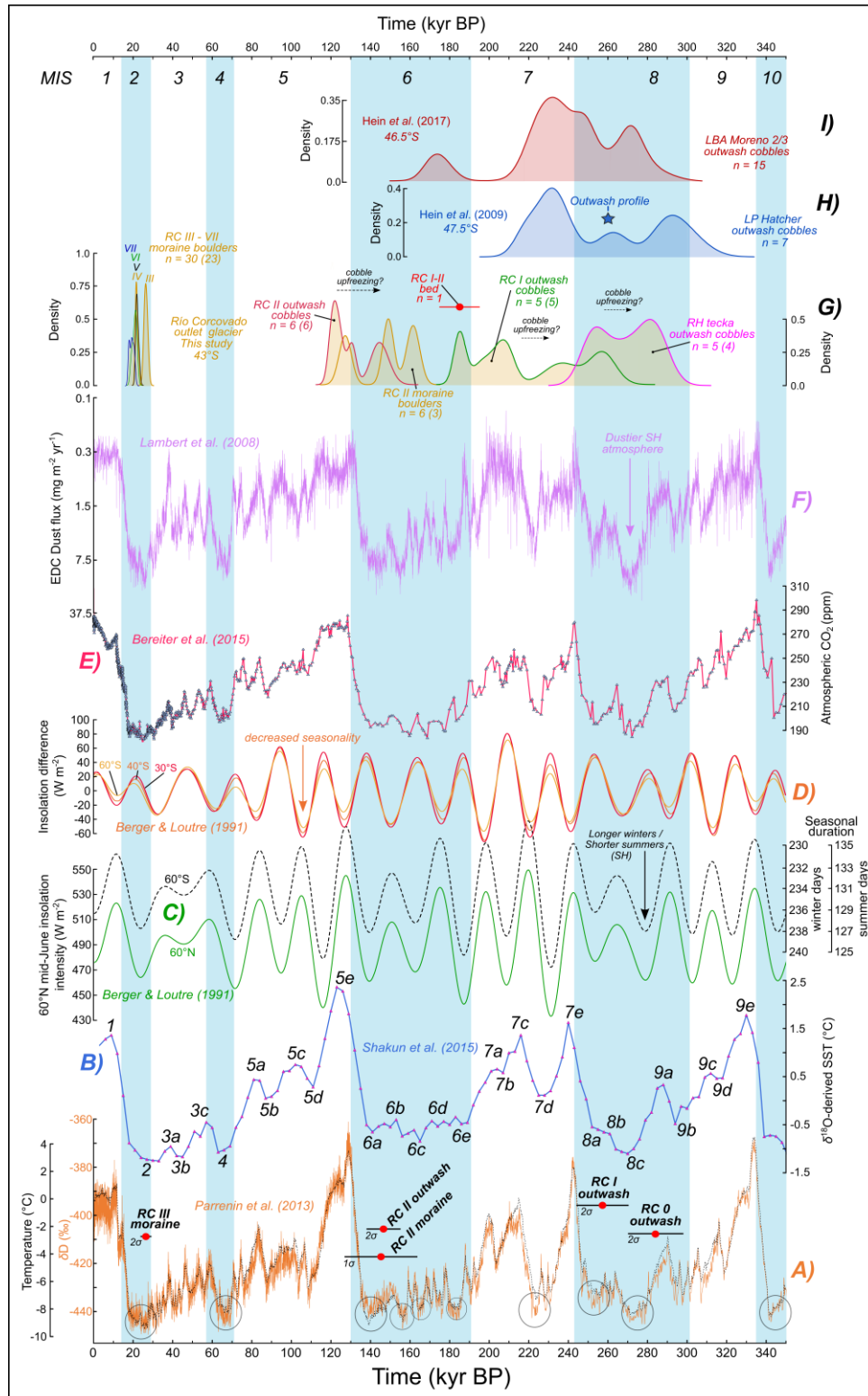
1095

1100

1105

1110

1115





1120 Figure 8. Vertical plot comparing this investigation's TCN ^{10}Be chronology to other Patagonian outlet-glacier TCN chronologies, to insolation intensity variations, and to palaeo-climate proxy records over the past 350 ka. (A) Stable isotope δ Deuterium record (orange curve) from the EPICA Dome C (EDC) ice core, 75°S, east-Antarctica and Antarctic atmospheric temperature (overlying dashed black curve) from a stack of isotopic temperature reconstructions from five different ice cores (EDC, Vostok, Dome Fuji, TALDICE, and EDML) (Parrenin *et al.*, 2013), with most potent cooling events of the past 350 ka highlighted by black circles. TCN exposure ages from the RC valley interpreted as best minimum-age estimate for each reconstructed glacial event are displayed (red dots) with analytical uncertainty (black horizontal bars). (B): Global stack ($n = 49$ cores) of paired planktonic $\delta^{18}\text{O}$ -derived Sea Surface Temperature (SST) data with Marine Isotope Stage numbers indicated (Shakun *et al.*, 2015). (C): Dark green line: summer (mid-June) insolation intensity for 60°N (Berger and Loutre, 1991). Dashed black curve: seasonal duration at 60°S (insolation threshold = 300 W m^{-2}) after Huybers and Denton (2008) and Denton *et al.* (2021). (D): Southern Hemisphere seasonality at 30°S, 40°S, and 60°S calculated by subtracting June from December insolation intensity values (Berger and Loutre, 1991), such that increasing seasonality indicates colder winters and warmer summers (after Darvill *et al.*, 2016). (E): Atmospheric CO_2 concentrations composite record from several Antarctic ice cores including EDC, WAIS, Vostock, Siple Dome, TALDICE, EDML, and LAW Dome (Bereiter *et al.*, 2015). (F): Dust flux record from the EDC ice core (Lambert *et al.*, 2008). (G-I): Kernel density distribution curves (1σ) for TCN exposure ages from the RC O – RC II moraine-outwash records (this study: G), the Hatcher moraine-outwash complex, in the Lago Cochrane/Pueyrredón valley (Hein *et al.*, 2009; H), and the Moreno 2/3 moraine-outwash limits, in the Lago General Carrera / Buenos Aires valley (Hein *et al.*, 2017; I).

1135

5.3 Climatic and orbital drivers of SH glaciations - hypotheses

Our chronology implies that the most extensive middle Pleistocene PIS expansion events preserved match the strongest
1140 minima in Antarctic atmospheric temperatures (Parrenin *et al.*, 2013), global oceanic SSTs (Shakun *et al.*, 2015), and global atmospheric CO_2 concentrations (Bereiter *et al.*, 2015) (Fig. 8). They also often appear to occur a few ka after minima in NH summer insolation intensity (60°N) and maxima in SH seasonality, while being out-of-phase with mid-latitude SH summer insolation intensity (Fig. 8c). The first observations of the asynchrony between SH mid-latitude glacier advances/recessions and local summer insolation intensity (*e.g.* Mercer, 1976; Denton *et al.*, 1999) encouraged the hypothesis that major glacial-
1145 termination-inducing warming signals were primarily controlled by NH summer insolation intensity driving NH glacial mass balance, and were propagated from the northern to the southern hemisphere through oceanic and atmospheric circulation shifts (*e.g.* Broecker, 1998; Denton *et al.*, 2010). Some of these interhemispheric climate-transmission mechanisms, such as the impact of the abrupt weakening of the Atlantic meridional overturning circulation in the north Atlantic following the last deglaciation, have been well documented (Barker *et al.*, 2009; Denton *et al.*, 2010). However, there is still a great deal of
1150 debate regarding the dominant trigger mechanisms responsible for global ice-sheet expansion/retreat cycles (Putnam *et al.*, 2013). Indeed, the above hypothesis entails the dilemma that while NH summer insolation intensity would be a key driver of NH ice-sheet mass balance, it would instead have little impact on mass fluctuations of SH mid-latitude ice sheets and



glaciers (Denton *et al.*, 2021). This problem invites the consideration of alternative hypotheses, such as the potential roles of SH seasonality and seasonal duration on controlling global ice-sheet mass fluctuations.

1155

García *et al.* (2018) noted that the extensive advances of the Torres del Paine (51°S) and the Última Esperanza (51.5°S) outlet glaciers at 48 ka (MIS 3) coincide with a minimum in obliquity-modulated high-latitude winter insolation intensity. The authors therefore hypothesise that colder SH winters during periods of high obliquity may favour SH mid-latitude glaciation by promoting local atmospheric cooling, Southern Ocean stratification and expanded Antarctic sea ice. Since we observe that middle-to-late Pleistocene PIS expansion events appear to occur during periods of longer, colder winters and shorter, warmer summers, we suggest that other PIS chronologies (including this study) may support García *et al.* (2018)'s hypothesis.

1160

Alternatively, the “Zealandia Switch” hypothesis (Denton *et al.*, 2021) focuses on the SH seasonal-duration aspect of orbitally-controlled insolation as a potential driver of late-Quaternary glaciation. By pacing the seasonal cycle of weakened and northward-migrated SWW during winter versus strengthened and southward-migrated SWW during summer, this hypothesis implies that SH seasonal duration might be a key driver of global climate change during middle-to-late Pleistocene glacial/interglacial cycles. Using global climate model simulations, the authors show that a reduced SH summer duration and increased SH winter duration could cause millennial-scale equatorward migrations of the SWW and its coupled Antarctic Circumpolar Current. Such zonal wind configuration would induce a northward migration of the subtropical front and a latitudinally-restricted subtropical gyre system in the Indo-Pacific Ocean basins (*ibid*). The bathymetry of the Australia/Zealandia continent is such that a restricted Indo-Pacific subtropical gyre could decrease Indonesian Throughflow and restrict westward Agulhas Leakage into the South Atlantic Ocean (Lorrey and Bostock, 2017). A reduced Agulhas Leakage has implications for the Atlantic salt input resulting in a potential weakening of Atlantic meridional overturning circulation (Caley *et al.*, 2012). The authors thus argue that such a southern oceanic and atmospheric circulation configuration could promote a global glacial mode (Denton *et al.*, 2021) that would greatly affect SH and thus Patagonian glacier mass balance.

1170

1175

Moreover, variations in the intensity and latitudinal position of the SWW influence Southern Ocean upwelling of deep-stored CO_2 and nutrients (Anderson *et al.*, 2009; Ai *et al.*, 2020). This mechanism is thought to represent a major contribution to variations in global atmospheric CO_2 concentrations over millennial timescales (Sarmiento and Toggweiler, 1984). Former equatorward shifts and weakening of the SWW could have decreased Southern Ocean upwelling and enhanced CO_2 storage in the deep ocean, thus causing delayed global cooling amplification (Sime *et al.*, 2013). Conversely, a poleward migration and strengthening of the SWW is thought to amplify global warming via increasing Southern Ocean upwelling, CO_2 outgassing and increasing CO_2 atmospheric concentrations. This hypothetical CO_2 capacitor storage-and-release mechanism may explain the highly amplified warming observed during major glacial terminations (Anderson *et al.*,

1185



2009; Denton *et al.*, 2021). This positive feedback mechanism may partly justify why middle-to-late Pleistocene global oceanic and atmospheric temperature variations often reached their most extreme values with some notable delay (a few ka) relative to NH mid-latitude summer insolation intensity.

1190

To summarise, empirical data including this study suggest that major middle-to-late Pleistocene cycles of SH mid-latitude glaciers and ice sheets appear to be coeval with NH glaciers and ice sheets, but out-of-phase with local mid-latitude summer insolation intensity (Putnam *et al.*, 2013; Peltier *et al.*, 2021), traditionally thought to be the primary driver of middle-to-late Pleistocene glacial expansion/demise cycles (Mercer, 1984). However, recent hypotheses suggest that this paradox might be explained by the potentially more dominant climate-forcing effect of the seasonality and seasonal-duration expressions of SH insolation, through their impact on atmospheric temperature, the position of the SWW belt and Subtropical Front, Antarctic sea ice extent, and Southern Ocean stratification and CO_2 storage-and-release feedback mechanisms. Testing the above hypotheses, and determining which of seasonality versus seasonal duration played a primary role in driving SH climate and glacial variations during the middle-to-late Pleistocene, represent key avenues for future research.

1195

1200

1205

1210

1215



6 Conclusions

- 1220 • We provide geomorphological and direct chronological evidence for at least three extensive, stratigraphically distinct pre-Last Glacial Cycle advances of the Río Corcovado glacier, a major outlet of the former northern Patagonian Ice Sheet. TCN surface exposure dating of outwash surface cobbles yields best minimum-age estimates for the RC 0, RC I and RC II advances of 284 ± 7 ka, 257 ± 7 ka, and 147 ± 4 ka, respectively.
- 1225 • Together with evidence we have reported in Leger *et al.* (2021a, b), our complete chronology reveals a minimum of four distinct expansion events of northeastern Patagonian Ice Sheet outlet glaciers that occurred during the MIS 8, MIS 6, and MIS 2 intervals. Further results gathered from bedrock surface and moraine boulder exposure ages also provide inceptive evidence for another MIS 7 expansion event and at least another MIS 6 advance previously reaching a close extent to that of the penultimate RC II advance.
- 1230 • Our dataset presents the first robust direct dating evidence of MIS 6 glaciations in Patagonia.
- 1235 • We did not find evidence for MIS 4 and 3 deposits in the RC valley geomorphological record. However, extensive glaciations did occur at these times on the former western margin of the Ice Sheet, and in other, more southern Patagonian regions. This highlights longitudinal and latitudinal asynchronies in former Patagonian Ice Sheet mass balance during these stages. We suggest that MIS 4 and 3 outlet-glacier advances likely occurred in northeastern Patagonia, but were of relatively shorter extent, and their associated deposits were likely eroded by the younger, more extensive MIS 2 glaciation.
- 1240 • We interpret that major middle-to-late Pleistocene Patagonian Ice Sheet expansions occurred in synchrony with the greatest cooling events recorded in global SST and Antarctic atmospheric temperatures, with the most prominent peaks in Antarctic ice-core dust concentrations, and with major minima in global CO_2 atmospheric concentrations. We observe a particularly good correlation between Antarctic atmospheric temperature signals and southern mid-latitude ice-sheet volume fluctuations, over several glacial cycles.
- 1245 • Our results suggest that Patagonian glaciations were more extensive during MIS 8 than during MIS 6-2, while global ice volumes and sea level depression were not particularly high during MIS 8. This implies that there was interhemispheric asynchrony in the relative volume and extent of Earth's major ice sheets during MIS 8. However, we acknowledge that a larger MIS 8 eastern Patagonian Ice Sheet is not necessarily indicative of a more potent local climate-forcing event than



1250 during younger glaciations (MIS 6-2) as glacial erosion, which greatly influences the local topography, may play a role in
controlling ice-sheet extent.

• Major middle-to-late Pleistocene advances of the Patagonian Ice Sheet appear to have occurred out-of-phase with local
summer insolation intensity but in synchrony with orbitally-controlled periods of longer and colder winters. We
1255 hypothesise that seasonality and seasonal duration may exert more control over southern mid-latitude ice-sheet mass
balance than mid-latitude summer insolation intensity over millennial timescales. This may be a consequence of the
possible effect of seasonal duration variability on the strength and migration of the SWW, and the impact of these
migrations on global climate and Southern Ocean circulation and CO_2 upwelling, as proposed by the “*Zealandia Switch*”
hypothesis.

1260 • Our findings corroborate work by Hein *et al.* (2009; 2017) and indicate that, in eastern Patagonia, pre-LGC outwash
surface cobbles yield exposure ages displaying less post-depositional scatter than moraine boulders from the same
margins, and hence facilitate more accurate estimations of the approximate timing of pre-LGC glacial advances.

1265

1270

1275



1280 **Data availability.**

All data associated with the production of new ^{10}Be and ^{26}Al TCN exposure ages, including sample characteristics and preparation protocols, are provided in the manuscript tables, figures, and the Supplementary Materials. Further inquiries can be directed to the corresponding author.

1285 **Data online repository.**

The data needed to re-calculate the ^{10}Be and ^{26}Al TCN exposure ages presented in this paper using the "online calculator formerly known as the CRONUS-Earth online calculators" version 3 is freely available online, as long as original publication is cited when used and/or referred to. This includes a textfile with data blocks in the correct input format and arranged by
1290 landforms studied in this investigation. The data are located in an open-access Mendeley Data online repository, accessible using this DOI: <https://doi.org/10.17632/gg4b3sh9k2.1>.

Team list.

1295 ASTER Team: Georges Aumaître (Aix-Marseille Université, CNRS, Coll. France, IRD, INRAE, CEREGE, Aix en Provence, 13545, France), Fawzi Zaidi (Aix-Marseille Université, CNRS, Coll. France, IRD, INRAE, CEREGE, Aix en Provence, 13545, France) and Karim Keddadouche (Aix-Marseille Université, CNRS, Coll. France, IRD, INRAE, CEREGE, Aix en Provence, 13545, France).

1300 **Author contributions.**

T.P.M.L co-concieved the study with A.S.H, raised the finances for fieldwork, conducted fieldwork with help from P.T.G, wrote NERC NEIF grant application together with A.S.H, conducted result analyses and interpretations, wrote the manuscript and supplementary materials with feedback from A.S.H. and R.G.B primarily, and A.R., I.S, and D.F. in a
1305 second time, and generated maps and figures. TCN exposure-age analyses including wet chemistry and AMS measurements were conducted by A.R and D.F at SUERC and T.P.M.L, I.S and the ASTER Team at CEREGE and the ASTER AMS.

Competing interest.

1310 We (the authors) hereby declare that this scientific investigation presents no known competing financial interests or personal conflicts influencing research output.

Disclaimer.



1315 **Acknowledgements.**

We express our gratitude towards all individuals who contributed to the <https://crowd.science/> crowdfunding campaign that provided us with the means to conduct a field expedition to the study site in January and February 2020. We thank all local landowners who authorized access and sampling on their properties, in particular, the Estancia Tecka (Chubut province, Argentina) for enabling access to their land and private roads. We thank Elaine McDougall and Allan Davidson for their invaluable laboratory work enabling efficient quartz isolation and purification from our rock samples.

Financial support.

1325 This study was conducted within the context of a University of Edinburgh E³ Doctoral Training Partnership Ph.D. studentship (award code: NE/L002558/1) awarded by the Natural Environment Research Council (NERC) and the University of Edinburgh School of GeoSciences to T.P.M.L. Fieldwork (01/02 2020) was partly supported by a crowdfunding campaign through the Crowd.Science fundraising platform (<https://crowd.science>) and a British Society for Geomorphology Postgraduate Research Grant award (BSG-2019-04) awarded to T.P.M.L. TCN exposure dating laboratory analysis and AMS measurements were funded by a NERC National Environmental Isotope Facility (NEIF) grant (2245-0320) awarded to A.S.H. and T.P.M.L. in July 2020.

Review statement.

1335

1340



References.

- 1345 **Ai**, X.E., Studer, A.S., Sigman, D.M., Martínez-García, A., Fripiat, F., Thöle, L. M., Michel, E., Gottschalk, J., Arnold, L., Moretti, S., Schmitt, M., Oleynik, S., Jaccard, S.L., and Haug, G.H., 2020, Southern Ocean upwelling, Earth's obliquity, and glacial-interglacial atmospheric CO₂ change: *Science*, v. 370(6522), p. 1348-1352, doi: <https://doi.org/10.1126/science.abd2115>.
- 1350 **Anderson**, R. F., Ali, S., Bradtmiller, L. I., Nielsen, S. H. H., Fleisher, M. Q., Anderson, B. E., and Burekle, L. H., 2009, Wind-driven upwelling in the Southern Ocean and the deglacial rise in atmospheric CO₂: *Science*, v. 323(5920), p. 1443-1448, doi: <https://doi.org/10.1126/science.1167441>.
- Astakhov**, V., 2011. Ice margins of northern Russia revisited. In: Ehlers, J., Gibbard, P.L., Hughes, P.D. (Eds.), *Quaternary Glaciations - Extent and Chronology: A Closer Look*. Developments in Quaternary Sciences 15. Elsevier, Amsterdam, pp. 1–14.
- 1355 **Astakhov**, V., Shkatova, V., Zastrozhnov, A., and Chuyko, M., 2016, Glaciomorphological map of the Russian Federation: *Quaternary International*, v. 420, p. 4-14, doi: <https://doi.org/10.1016/j.quaint.2015.09.024>.
- Augustinus**, P., Fink, D., Fletcher, M. S., and Thomas, I., 2017, Re-assessment of the mid to late Quaternary glacial and environmental history of the Boco Plain, western Tasmania: *Quaternary Science Reviews*, v. 160, p. 31-44, doi: <https://doi.org/10.1016/j.quascirev.2017.01.015>.
- 1360 **Balco**, G., 2006, Converting Al and Be isotope ratio measurements to nuclide concentrations in quartz, Documentation—Be-10/26-Al exposure age calculator.
- Balco**, G., and Rovey, C. W., 2008, An isochron method for cosmogenic-nuclide dating of buried soils and sediments. *American Journal of Science*, v. 308(10), p. 1083-1114, doi: <https://doi.org/10.2475/10.2008.02>.
- 1365 **Balco**, G., Stone, J.O., Lifton, N.A., and Dunai, T.J., 2008, A complete and easily accessible means of calculating surface exposure ages or erosion rates from 10Be and 26Al measurements: *Quaternary geochronology*, v. 3(3), p. 174-195, doi: <https://doi.org/10.1016/j.quageo.2007.12.001>.
- Barker**, S., Diz, P., Vautravers, M. J., Pike, J., Knorr, G., Hall, I. R., and Broecker, W. S., 2009, Interhemispheric Atlantic seesaw response during the last deglaciation: *Nature*, v. 457(7233), p. 1097-1102, doi: <https://doi.org/10.1038/nature07770>.
- 1370 **Barrows**, T. T., Stone, J. O., Fifield, L. K., and Cresswell, R. G., 2002, The timing of the last glacial maximum in Australia: *Quaternary Science Reviews*, v. 21(1-3), p. 159-173: doi: [https://doi.org/10.1016/S0277-3791\(01\)00109-3](https://doi.org/10.1016/S0277-3791(01)00109-3).
- Beets**, D.J., Meijer, T., Beets, C.J., Cleveringa, P., Laban, C., and Van der Spek, A.J.F., 2005, Evidence for a Middle Pleistocene glaciation of MIS 8 age in the southern North Sea: *Quaternary International*, v. 133, p. 7-19, doi: <https://doi.org/10.1016/j.quaint.2004.10.002>.



- 1375 **Bereiter**, B., Eggleston, S., Schmitt, J., Nehrbass-Ahles, C., Stocker, T. F., Fischer, H., Kipfstuhl, S., Chappellaz, J., 2015, Revision of the EPICA Dome C CO₂ record from 800 to 600 kyr before present: *Geophysical Research Letters*, v. 42(2), p. 542-549, doi: <https://doi.org/10.1002/2014GL061957>.
- Berger**, A., and Loutre, M.F., 1991, Insolation values for the climate of the last 10 million years: *Quaternary Science Reviews*, v. 10(4), p. 297-317, doi: [https://doi.org/10.1016/0277-3791\(91\)90033-Q](https://doi.org/10.1016/0277-3791(91)90033-Q).
- 1380 **Borchers**, B., Marrero, S., Balco, G., Caffee, M., Goehring, B., Lifton, N., Nishiizumi, K., Phillips, F., Schaefer, J., and Stone, J., 2016, Geological calibration of spallation production rates in the CRONUS-Earth project: *Quaternary Geochronology*, v. 31, p. 188-198. Doi: <https://doi.org/10.1016/j.quageo.2015.01.009>.
- Briner**, J. P., Kaufman, D. S., Manley, W. F., Finkel, R. C., and Caffee, M. W., 2005, Cosmogenic exposure dating of late Pleistocene moraine stabilization in Alaska: *Geological Society of America Bulletin*, v. 117(7-8), p. 1108-1120, doi: <https://doi.org/10.1130/B25649.1>.
- 1385 **Broecker**, W.S., 1998, Paleocean circulation during the last deglaciation: a bipolar seesaw?: *Paleoceanography*, v. 13 (2), p. 119-121, doi: <https://doi.org/10.1029/97PA03707>.
- Caldenius**, C.C.Z., 1932, Las glaciaciones cuaternarias en la patagonia y tierra del fuego: *Geografiska Annaler*, v.14, p. 1–164, doi: <https://doi.org/10.1080/20014422.1932.11880545>.
- 1390 **Caley**, T., Giraudeau, J., Malaizé, B., Rossignol, L., and Pierre, C., 2012, Agulhas leakage as a key process in the modes of Quaternary climate changes: *Proceedings of the National Academy of Sciences*, v. 109(18), p. 6835-6839, doi: <https://doi.org/10.1073/pnas.1115545109>.
- Clapperton**, C.M., 1993, *Quaternary geology and geomorphology of South America*: Amsterdam, Elsevier Science Publishers B.V., 779 p.
- 1395 **Cogez**, A., Herman, F., Pelt, É., Reuschlé, T., Morvan, G., Darvill, C. M., Norton, K. P., Christl, M., Märki, L., Chabaux, F., 2018, U–Th and 10 Be constraints on sediment recycling in proglacial settings, Lago Buenos Aires, Patagonia: *Earth Surface Dynamics*, v. 6(1), p. 121-140, doi: <https://doi.org/10.5194/esurf-6-121-2018>.
- Colhoun**, E.A., Barrows, T.T., 2011. The glaciation of Australia. In: Ehlers, J., Gibbard, P.L., Hughes, P.D. (Eds.), *Quaternary Glaciations - Extent and Chronology: A Closer Look*. *Developments in Quaternary Sciences 15*. Elsevier, Amsterdam, pp. 1037–1045.
- 1400 **Darvill**, C. M., Bentley, M. J., Stokes, C. R., Hein, A. S., and Rodés, Á, 2015, Extensive MIS 3 glaciation in southernmost Patagonia revealed by cosmogenic nuclide dating of outwash sediments: *Earth and Planetary Science Letters*, v. 429, p. 157-169, doi: <https://doi.org/10.1016/j.epsl.2015.07.030>.
- Darvill**, C. M., Bentley, M. J., Stokes, C. R., and Shulmeister, J., 2016, The timing and cause of glacial advances in the southern mid-latitudes during the last glacial cycle based on a synthesis of exposure ages from Patagonia and New Zealand: *Quaternary Science Reviews*, v. 149, p. 200-214, doi: <https://doi.org/10.1016/j.quascirev.2016.07.024>.
- 1405 **Davies**, B. J., Roberts, D.H., Bridgland, D.R., Cofaigh, C.Ó., Riding, J.B., Demarchi, B., Penkman, K.E.H., and Pawley, S. M., 2012, Timing and depositional environments of a Middle Pleistocene glaciation of northeast England: *New evidence*



- from Warren House Gill, County Durham: *Quaternary Science Reviews*, v. 44, p. 180-212.
1410 <https://doi.org/10.1016/j.quascirev.2010.02.003>.
- Davies**, B. J., Darvill, C. M., Lovell, H., Bendle, J. M., Dowdeswell, J. A., Fabel, D., Garcia, J-L., Geiger, A., Glasser, N. F., Gheorghiu, D. M., Harrison, S., Hein, A. S., Kaplan, M. R., Martin, J. R. V., Mendelova, M., Palmer, A., Pelto, M., Rodes, A., Sagredo, E. A., Smedley, R., Smellie, J. L., and Thorndycraft, V. R., 2020, The evolution of the Patagonian Ice Sheet from 35 ka to the Present Day (PATICE): *Earth-Science Reviews*, 103152, doi:
1415 <https://doi.org/10.1016/j.earscirev.2020.103152>.
- Denton**, G.H., Lowell, T.V., Heusser, C.J., Schlüchter, C., Andersen, B.G., Heusser, L.E., Moreno, P.I., Marchant, D.R., 1999. Geomorphology, stratigraphy, and radio- carbon chronology of llanquihue drift in the area of the southern lake district, Seno reloncaví, and Isla grande de Chiloé, Chile: *Geografiska Annaler, Series A, Physical Geography*, v. 81 (2), p. 167-229, doi: <https://doi.org/10.1111/j.0435-3676.1999.00057.x>.
- 1420 **Denton**, G.H., Anderson, R.F., Toggweiler, J.R., Edwards, R.L., Schaefer, J.M., and Putnam, A.E., 2010, The last glacial termination: *Science*, v. 328, p. 1652-1656, doi: <https://doi.org/10.1126/science.1184119>.
- Denton**, G.H., Putnam, A.E., Russell, J.L., Barrell, D.J., Schaefer, J.M., Kaplan, M.R., and Strand, P.D., 2021, The Zealandia Switch: Ice age climate shifts viewed from Southern Hemisphere moraines: *Quaternary Science Reviews*, v. 257, 106771, doi: <https://doi.org/10.1016/j.quascirev.2020.106771>.
- 1425 **Douglass**, D.C., Singer, B.S., Ackert, R.P., Kaplan, M.R., and Caffee, M.W, 2007, Constraining Boulder Erosion Rates and Ages of Mid-Pleistocene Moraines. Lago Buenos Aires, Argentina. Geological Society of America Abstracts and Programs, Northeastern Section, 42nd Annual Meeting.
- Evans**, D.J.A., Roberts, D.H., Bateman, M.D., Ely, J., Medialdea, A., Burke, M.J., Chiverrell, R.C., Clark, C.D., Fabel, D., 2019, A chronology for North Sea Lobe advance and recession on the Lincolnshire and Norfolk coasts during MIS 2 and 6: *Proceedings of the Geologists' Association*, v.130, p. 523–540, doi: <https://doi.org/10.1016/j.pgeola.2018.10.004>.
- 1430 **Fernandes**, M., Oliva, M., Vieira, G., Palacios, D., Fernández-Fernández, J. M., Delmas, M., García-Oteyza, J., Schimmelpfennig, I., Ventura, J., ASTER Team., 2021, Maximum glacier extent of the Penultimate Glacial Cycle in the Upper Garonne Basin (Pyrenees): new chronological evidence: *Environmental Earth Sciences*, v. 80(24), p. 1-20, doi: <https://doi.org/10.1007/s12665-021-10022-z>.
- 1435 **Fick**, S. E., and Hijmans, R. J., 2017, WorldClim 2: new 1-km spatial resolution climate surfaces for global land areas: *International journal of climatology*, v. 37(12), p. 4302-4315. doi: <https://doi.org/10.1002/joc.5086>.
- García**, J. L., Hein, A. S., Binnie, S. A., Gómez, G. A., González, M. A., and Dunai, T. J., 2018, The MIS 3 maximum of the Torres del Paine and Última Esperanza ice lobes in Patagonia and the pacing of southern mountain glaciation: *Quaternary Science Reviews*, v. 185, p. 9-26, doi: <https://doi.org/10.1016/j.quascirev.2018.01.013>.
- 1440 **García**, J. L., Lüthgens, C., Vega, R. M., Rodés, Á., Hein, A. S., and Binnie, S., 2021, A composite 10Be, IR-50 and 14C chronology of the pre-LGM full ice extent of the western Patagonian Ice Sheet in the Isla de Chiloé, south Chile (42°S): *E&G Quaternary Science Journal*, v. 70, p. 105–128, doi: <https://doi.org/10.5194/egqsj-70-105-2021>.



- Garreaud**, R., Lopez, P., Minvielle, M., and Rojas, M., 2013, Large-scale control on the Patagonian climate: *Journal of Climate*, v. 26(1), p. 215-230, doi: <https://doi.org/10.1175/JCLI-D-12-00001.1>.
- 1445 **Glasser**, N., and Jansson, K., 2008, The glacial map of southern South America: *Journal of Maps*, v. 4(1), p. 175-196, doi: <https://doi.org/10.4113/jom.2008.1020>.
- Gómez**, G. A., García, J. L., Villagrán, C., Lüthgens, C., Abarzúa, A. M., 2022, Vegetation, glacier, and climate changes before the global last glacial maximum in the Isla Grande de Chiloé, southern Chile (42° S): *Quaternary Science Reviews*, v. 276, 107301, doi: <https://doi.org/10.1016/j.quascirev.2021.107301>.
- 1450 **Gosse**, J. C., and Phillips, F. M., 2001, Terrestrial in situ cosmogenic nuclides: theory and application: *Quaternary Science Reviews*, v. 20(14), p. 1475-1560, doi: [https://doi.org/10.1016/S0277-3791\(00\)00171-2](https://doi.org/10.1016/S0277-3791(00)00171-2).
- Granger**, D. E., and Muzikar, P. F., 2001, Dating sediment burial with in situ-produced cosmogenic nuclides: theory, techniques, and limitations. *Earth and Planetary Science Letters*, v. 188(1-2), p. 269-281, doi: [https://doi.org/10.1016/S0012-821X\(01\)00309-0](https://doi.org/10.1016/S0012-821X(01)00309-0).
- 1455 **Haller**, M., Lech, R.R., Martinez, O.A., Meister, C.M., and Page, S.M., 2003, Hoja Geologica 4373IV/III, Trevelin, Provincia del Chubut. Programa Nacional de Cartas Geologicas de la Republica Argentina: Servicio Geologico Nacional, Buenos Aires, scale 1:250.000.
- Hein**, A. S., Hulton, N. R., Dunai, T. J., Schnabel, C., Kaplan, M. R., Naylor, M., and Xu, S., 2009, Middle Pleistocene glaciation in Patagonia dated by cosmogenic-nuclide measurements on outwash gravels: *Earth and Planetary Science Letters*, v. 286(1-2), p. 184-197, doi: <https://doi.org/10.1016/j.epsl.2009.06.026>.
- 1460 **Hein**, A. S., Dunai, T. J., Hulton, N. R., and Xu, S., 2011, Exposure dating outwash gravels to determine the age of the greatest Patagonian glaciations: *Geology*, v. 39(2), p. 103-106, doi: <https://doi.org/10.1130/G31215.1>.
- Hein**, A.S., Cogez, A., Darvill, C.M., Mendelová, M., Kaplan, M.R., Herman, F., Dunai, T.J., Norton, K., Xu, S., Christl, M., and Rodés, Á., 2017, Regional mid-Pleistocene glaciation in central Patagonia: *Quaternary Science Reviews*, v. 164, p. 77-94, doi: <https://doi.org/10.1016/j.quascirev.2017.03.023>.
- 1465 **Hervé**, F., Fuentes, F., Calderón, M., Fanning, M., Quezada, P., Pankhurst, R., and Rapela, C., 2017, Ultramafic rocks in the North Patagonian Andes: is their emplacement associated with the Neogene tectonics of the Liquiñe-Ofqui Fault Zone?: *Andean Geology*, v. 44(1), P. 1-16, doi: <https://doi.org/10.5027/andgeoV44n1-a01>.
- Hughes**, P. D., Gibbard, P. L., and Ehlers, J., 2020, The “missing glaciations” of the Middle Pleistocene: *Quaternary Research*, v. 96, p. 161-183, doi: <https://doi.org/10.1017/qua.2019.76>
- 1470 **Huybers**, P., Denton, G., 2008, Antarctic temperature at orbital timescales controlled by local summer duration. *Nature Geoscience*. v. 1, p.787-792, doi: <https://doi.org/10.1038/ngeo311>.
- Jones**, R.S., Small, D., Cahill, N., Bentley, M.J., and Whitehouse, P.L., 2019, iceTEA: Tools for plotting and analysing cosmogenic-nuclide surface-exposure data from former ice margins: *Quaternary Geochronology*, v. 51, p. 72-86, doi: <https://doi.org/10.1016/j.quageo.2019.01.001>.
- 1475



- Kaplan**, M.R., Douglass, D.C., Singer, B.S., and Caffee, M.W., 2005, Cosmogenic nuclide chronology of pre-last glacial maximum moraines at Lago Buenos Aires, 46 degrees S, Argentina: *Quaternary Research*, v. 63, p. 301–315, doi: <https://doi.org/10.1016/j.yqres.2004.12.003>
- 1480 **Kaplan**, M. R., Hein, A. S., Hubbard, A., & Lax, S. M, 2009, Can glacial erosion limit the extent of glaciation?: *Geomorphology*, v. 103(2), p. 172-179, doi: <https://doi.org/10.1016/j.geomorph.2008.04.020>.
- Kaplan**, M.R., Schaefer, J.M., Denton, G.H., Barrell, D.J., Chinn, T.J., Putnam, A.E., Andersen, B.G., Finkel, R.C., Schwartz, R., and Doughty, A.M, 2010, Glacier retreat in New Zealand during the Younger Dryas stadial: *Nature*, V. 467(7312), p. 194-197, doi: <https://doi.org/10.1038/nature09313>.
- 1485 **Kaplan**, M.R., Strelin, J.A., Schaefer, J.M., Denton, G.H., Finkel, R.C., Schwartz, R., Putnam, A.E., Vandergoes, M.J., Goehring, B.M., and Travis, S.G., 2011, In-situ cosmogenic ^{10}Be production rate at Lago Argentino, Patagonia: implications for late-glacial climate chronology: *Earth and Planetary Science Letters*, v. 309(1-2), p. 21-32, doi: <https://doi.org/10.1016/j.epsl.2011.06.018>.
- Kiernan**, K., Fifield, L. K., & Chappell, J., 2004, Cosmogenic nuclide ages for last glacial maximum moraine at Schnells Ridge, southwest Tasmania: *Quaternary Research*, v. 61(3), p. 335-338, doi: <https://doi.org/10.1016/j.yqres.2004.02.004>.
- 1490 **Kiernan**, K., Fink, D., Greig, D., & Mifud, C., 2010, Cosmogenic radionuclide chronology of pre-last glacial cycle moraines in the Western Arthur range, Southwest Tasmania: *Quaternary Science Reviews*, v. 29(23-24), p. 3286-3297, doi: <https://doi.org/10.1016/j.quascirev.2010.07.023>.
- Kiernan**, K., McMinn, M. S., and Fink, D., 2014, Topographic and microclimatic impacts on glaciation of the Denison Range, southwest Tasmania: *Quaternary Science Reviews*, v. 97, p. 136-147, doi: <https://doi.org/10.1016/j.quascirev.2014.05.008>.
- 1495 **Kiernan**, K., Fink, D., & McConnell, A., 2017, Cosmogenic ^{10}Be and ^{26}Al exposure ages of glaciations in the Frankland Range, southwest Tasmania reveal a limited MIS-2 ice advance: *Quaternary Science Reviews*, v. 157, p. 141-151, doi: <https://doi.org/10.1016/j.quascirev.2016.12.008>.
- Koffman**, B. G., Goldstein, S. L., Winckler, G., Borunda, A., Kaplan, M. R., Bolge, L., Cai, Y., Recasens, C., Koffman, T.N.B., and Vallelonga, P., 2021, New Zealand as a source of mineral dust to the atmosphere and ocean: *Quaternary Science Reviews*, v. 251, 106659, doi: <https://doi.org/10.1016/j.quascirev.2020.106659>.
- 1500 **Lal**, D., 1991, Cosmic ray labeling of erosion surfaces: in situ nuclide production: *Earth and Planetary Science Letters*, v. 104, p. 424-439, doi: [https://doi.org/10.1016/0012-821X\(91\)90220-C](https://doi.org/10.1016/0012-821X(91)90220-C).
- Lambeck**, K., Rouby, H., Purcell, A., Sun, Y., and Sambridge, M., 2014, Sea level and global ice volumes from the Last Glacial Maximum to the Holocene: *Proceedings of the National Academy of Sciences*, v. 111(43), p. 15296–15303. doi: <https://doi.org/10.1073/pnas.1411762111>.
- 1505 **Lambert**, F., Delmonte, B., Petit, J.R., Bigler, M., Kaufmann, P.R., Hutterli, M.A., Stocker, T.F., Ruth, U., Steffensen, J.P., Maggi, V., 2008, Dust-climate couplings over the past 800,000 years from the EPICA Dome C ice core: *Nature*, v. 452(7187), p. 616-619, doi: <https://doi.org/10.1038/nature06763>.



- 1510 **Lambert, F.**, Bigler, M., Steffensen, J.P., Hutterli, M., Fischer, H., 2012, Centennial mineral dust variability in high-resolution ice core data from Dome C, Antarctica: *Climate of the Past*, v. 8, p. 609–623, doi: <https://doi.org/10.5194/cp-8-609-2012>.
- Leger, T.P.M.**, Hein, A.S., Bingham, R.G., Martini, M.A., Rodrigo, L.S., Sagredo, E.A., and Martínez, O.A., 2020, The glacial geomorphology of the Río Corcovado, Río Huemul and Lago Palena/General Vintter valleys, northeastern Patagonia (43°S, 71°W): *Journal of Maps*, v. 16(2), p. 651–668, doi: <https://doi.org/10.1080/17445647.2020.1794990>.
- 1515 **Leger, T.P.M.**, Hein, A.S., Bingham, R.G., Rodés, Á., Fabel, D., and Smedley, R., 2021a, Geomorphology and ¹⁰Be chronology of the Last Glacial Maximum and deglaciation in northeastern Patagonia, 43°S–71°W: *Quaternary Science Reviews*, v. 272, doi: <https://doi.org/10.1016/j.quascirev.2021.107194>.
- Leger, T.P.M.**, Hein, A.S., Goldberg, D., Schimmelpfennig, I., Van Wyk de Vries, M.S., Bingham, R.G., and ASTER Team, 2021b, Northeastern Patagonian Glacier Advances (43°S) Reflect Northward Migration of the Southern Westerlies Towards the End of the Last Glaciation: *Frontiers in Earth Science*, v. 9, 751987, doi: <https://doi.org/10.3389/feart.2021.751987>.
- 1520 **Lifton, N.**, Sato, T., & Dunai, T. J., 2014, Scaling in situ cosmogenic nuclide production rates using analytical approximations to atmospheric cosmic-ray fluxes: *Earth and Planetary Science Letters*, v. 386, p. 149–160, doi: <https://doi.org/10.1016/j.epsl.2013.10.052>.
- 1525 **Lindner, L.**, and Marks, L., 1999, New approach to stratigraphy of palaeolake and glacial sediments of the younger Middle Pleistocene in mid-eastern Poland: *Geological Quarterly*, v. 43(1), p. 1–8.
- Lisiecki, L. E.**, and Raymo, M. E., 2005, A Pliocene–Pleistocene stack of 57 globally distributed benthic δ18O records. *Paleoceanography*, v. 20(1), doi: <https://doi.org/10.1029/2004PA001071>.
- Lorrey, A.M.**, Bostock, H., 2017, The Quaternary climate of New Zealand. *Advances in Quaternary Science - the New Zealand Landscape*. Springer-Verlag, pp. 67–139.
- 1530 **Margari, V.**, Skinner, L.C., Hodell, D.A., Martrat, B., Toucanne, S., Grimalt, J.O., Gibbard, P.L., Lunkka, J.P., and Tzedakis, P.C., 2014, Land-ocean changes on orbital and millennial time scales and the penultimate glaciation: *Geology*, v. 42, p. 183–186, doi: <https://doi.org/10.1130/G35070.1>.
- Martin, L. C. P.**, Blard, P. H., Balco, G., Lavé, J., Delunel, R., Lifton, N., and Laurent, V., 2017, The CREp program and the ICE-D production rate calibration database: A fully parameterizable and updated online tool to compute cosmic-ray exposure ages: *Quaternary geochronology*, v. 38, p. 25–49, doi: <https://doi.org/10.1016/j.quageo.2016.11.006>.
- 1535 **Meglioli, A.**, 1992, Glacial geology and chronology of southernmost Patagonia and Tierra del Fuego, Argentina and Chile [Ph.D. thesis]: Bethlehem, Pennsylvania, Lehigh University, 216 p.
- Mendelová, M.**, Hein, A. S., Rodés, Á., & Xu, S., 2020, Extensive mountain glaciation in central Patagonia during Marine Isotope Stage 5: *Quaternary Science Reviews*, v. 227, 105996, doi: <https://doi.org/10.1016/j.quascirev.2019.105996>.
- 1540 **Mercer, J.H.**, 1976, Glacial history of southernmost South America: *Quaternary Research*, v. 6, p. 125–166, doi: [https://doi.org/10.1016/0033-5894\(76\)90047-8](https://doi.org/10.1016/0033-5894(76)90047-8).



- Mercer**, J. H., 1984, Simultaneous climatic change in both hemispheres and similar bipolar interglacial warming: Evidence and implications: *Climate processes and climate sensitivity*, v. 29, p. 307-313, doi: <https://doi.org/10.1029/GM029p0307>.
- 1545 **Parrenin**, F., Masson-Delmotte, V., Köhler, P., Raynaud, D., Paillard, D., Schwander, J., Barbante, C., Landais, A., Wegner, A., and Jouzel, J., 2013, Synchronous change of atmospheric CO₂ and Antarctic temperature during the last deglacial warming: *Science*, v. 339(6123), p. 1060-1063. doi: <https://doi.org/10.1126/science.1226368>.
- Peltier**, C., Kaplan, M. R., Schaefer, J. M., Araos, J., Sagredo, E. A., and Schwartz, R., 2017 (December), Glacier-Climatic Change in Southern South America over Multiple Glacial Cycles and Implications for Glacial to Interglacial Shifts in the Westerly Winds: In 2017 AGU Fall Meeting. AGU, Bibcode: 2017AGUFMPP43B1349P
- 1550 **Peltier**, C., Kaplan, M.R., Birkel, S.D., Soteres, R.L., Sagredo, E.A., Aravena, J.C., Araos, J., Moreno, P.I., Schwartz, R., and Schaefer, J.M., 2021, A large MIS 4 and long MIS 2 glacier maximum on the southern tip of South America: *Quaternary Science Reviews*, v. 262, 106858, doi: <https://doi.org/10.1016/j.quascirev.2021.106858>.
- Phillips**, F.M., Zreda, M.G., Smith, S.S., Elmore, D., Kubik, P.W., and Sharma, P., 1990, Cosmogenic chlorine-36 chronology for glacial deposits at Bloody Canyon, eastern Sierra Nevada: *Science*, v. 248, p. 1529–1532, doi: <https://doi.org/10.1126/science.248.4962.1529>.
- 1555 **Preusser**, F., Graf, H. R., Keller, O., Krayss, E., & Schlüchter, C., 2011, Quaternary glaciation history of northern Switzerland: *E&G Quaternary Science Journal*, v. 60(2/3), p. 282-305, doi: <https://doi.org/10.3285/eg.60.2-3.06>.
- Putkonen**, J., and Swanson, T., 2003, Accuracy of cosmogenic ages for moraines: *Quaternary Research*, v. 59(2), p. 255-261, doi: [https://doi.org/10.1016/S0033-5894\(03\)00006-1](https://doi.org/10.1016/S0033-5894(03)00006-1).
- 1560 **Putnam**, A. E., Schaefer, J. M., Barrell, D. J. A., Vandergoes, M., Denton, G. H., Kaplan, M. R., Finkel, R. C., Schwartz, R., Goehring, B. M., and Kelley, S. E., 2010, In situ cosmogenic ¹⁰Be production-rate calibration from the Southern Alps, New Zealand: *Quaternary Geochronology*, v. 5(4), p. 392-409, doi: <https://doi.org/10.1016/j.quageo.2009.12.001>.
- Putnam**, A.E., Schaefer, J.M., Denton, G.H., Barrell, D.J.A., Birkel, S.D., Andersen, B.G., Kaplan, M.R., Finkel, R.C., Schwartz, R., and Doughty, A.M., 2013, The Last Glacial Maximum at 44°S documented by a ¹⁰Be moraine chronology at Lake Ohau, Southern Alps of New Zealand. *Quaternary Science Reviews*, v. 62, 114e141, doi: <https://doi.org/10.1016/j.quascirev.2012.10.034>.
- 1565 **Rabassa**, J., and Clapperton, C. M., 1990, Quaternary glaciations of the southern Andes: *Quaternary Science Reviews*, v. 9(2-3), p. 153-174, doi: [https://doi.org/10.1016/0277-3791\(90\)90016-4](https://doi.org/10.1016/0277-3791(90)90016-4).
- 1570 **Rabassa**, J., and Coronato, A., 2009, Glaciations in Patagonia and Tierra del Fuego during the Ensenadan stage/age (early Pleistocene–earliest middle Pleistocene): *Quaternary International*, v. 210(1-2), p. 18-36, doi: <https://doi.org/10.1016/j.quaint.2009.06.019>.
- Sarmiento**, J. L., and Toggweiler, J. R., 1984, A new model for the role of the oceans in determining atmospheric p CO₂: *Nature*, v. 308(5960), p. 621-624, doi: <https://doi.org/10.1038/308621a0>.
- 1575 **Schaefer**, J.M., Putnam, A.E., Denton, G.H., Kaplan, M.R., Birkel, S., Doughty, A.M., Kelley, S.E., Barrell, D.J.A., Finkel, R.C., Winckler, G., Anderson, R.F., Ninneman, U.S., Barker, S., Schwartz, R., Andersen, B.J., and Schluechter, C., 2015,



- The southern glacial maximum 65,000 years ago and its unfinished termination: *Quaternary Science Reviews*, v. 114, p. 52-60, doi: <https://doi.org/10.1016/j.quascirev.2015.02.009>.
- 1580 **Shakun**, J.D., Lea, D.W., Lisiecki, L.E., and Raymo, M. E., 2015, An 800-kyr record of global surface ocean $\delta^{18}\text{O}$ and implications for ice volume-temperature coupling: *Earth and Planetary Science Letters*, v. 426, p. 58-68, doi: <https://doi.org/10.1016/j.epsl.2015.05.042>.
- Sime**, L. C., Kohfeld, K. E., Le Quéré, C., Wolff, E. W., de Boer, A. M., Graham, R. M., and Bopp, L., 2013, Southern Hemisphere westerly wind changes during the Last Glacial Maximum: model-data comparison: *Quaternary Science Reviews*, v. 64, p. 104-120, doi: <https://doi.org/10.1016/j.quascirev.2012.12.008>.
- 1585 **Singer**, B.S., Brown, L.L., Rabassa, J.O. and Guillou, H., 2004, 40Ar/39Ar chronology of Late Pliocene and Early Pleistocene geomagnetic and glacial events in southern Argentina: In *Timescales Of The Paleomagnetic Field* (eds J. Channell, D. Kent, W. Lowrie and J. Meert), doi: <https://doi.org/10.1029/145GM13>.
- Spratt**, R.M., and Lisiecki, L.E., 2016, A Late Pleistocene sea level stack: *Climate of the Past*, v. 12(4), p. 1079-1092, doi: <https://doi.org/10.5194/cp-12-1079-2016>.
- 1590 **Stone**, J. O., 2000, Air pressure and cosmogenic isotope production: *Journal of Geophysical Research: Solid Earth*, v. 105(B10), p. 23753-23759, doi: <https://doi.org/10.1029/2000jb900181>.
- Sugden**, D.E., McCulloch, R.D., Bory, A.J.M., and Hein, A.S, 2009, Influence of Patagonian glaciers on Antarctic dust deposition during the last glacial period: *Nature Geoscience*, v. 2(4), p. 281-285, doi: <https://doi.org/10.1038/ngeo474>.
- Sylwan**, C., Beraza, L., and Caselli, A., 1991, Magnetoestratigrafía de la secuencia morenica en el valle del Lago Pueyrredon, provincia de Santa Cruz: *Revista de la Asociación Geológica Argentina*, v. 46, p. 235-238.
- 1595 **Terrizzano**, C. M., Morabito, E. G., Christl, M., Likerman, J., Tobal, J., Yamin, M., & Zech, R., 2017, Climatic and Tectonic forcing on alluvial fans in the Southern Central Andes: *Quaternary science reviews*, v. 172, p. 131-141, doi: <https://doi.org/10.1016/j.quascirev.2017.08.002>.
- Toucanne**, S., Zaragosi, S., Bourillet, J.F., Cremer, M., Eynaud, F., Van Vliet-Lanoe, B., Penaud, A., Fontanier, C., Turon, J.L., Cortijo, E., and Gibbard, P.L., 2009, Timing of massive “Fleuve Manche” discharges over the last 350 kyr: insights into the European ice-sheet oscillations and the European drainage network from MIS 10 to 2: *Quaternary Science Reviews*, v. 28, p. 1238-1256, doi: <https://doi.org/10.1016/j.quascirev.2009.01.006>.
- 1600 **Trombotto**, D., 2008, Geocryology of southern South America, in Rabassa, J., ed., *The late Cenozoic of Patagonia and Tierra del Fuego: Developments in Quaternary Sciences Volume 11*: Amsterdam, Elsevier, p. 255-268, doi: [https://doi.org/10.1016/S1571-0866\(07\)10012-9](https://doi.org/10.1016/S1571-0866(07)10012-9).
- 1605 **White**, T.S., Bridgland, D.R., Howard, A.J., Westaway, R., and White, M.J., 2010, Evidence from the Trent terrace archive, Lincolnshire, UK, for lowland glaciation of Britain during the Middle and Late Pleistocene: *Proceedings of the Geologists’ Association*, v. 121, p. 141-153, doi: <https://doi.org/10.1016/j.pgeola.2010.05.001>.



1610 **White, T.S., Bridgland, D.R., Westaway, R., and Straw, A., 2017, Evidence for late Middle Pleistocene glaciation of the**
British margin of the southern North Sea: *Journal of Quaternary Science*, v. 32(2), p. 261-275, doi:
<https://doi.org/10.1002/jqs.2826>.

1615